Research Paper

GEOSPHERE

GEOSPHERE, v. 20, no. 1

https://doi.org/10.1130/GES02650.1

7 figures; 1 table; 1 set of supplemental files

CORRESPONDENCE: stacey.gerasimov@yale.edu

CITATION: Gerasimov, S.H., Hodgin, E.B., Crowley, J.L., and Swanson-Hysell, N.L., 2024, Chronostratigraphy of Miocene strata in the Berkeley Hills (California Coast Ranges, USA) and the arrival of the San Andreas transform boundary: Geosphere, v. 20, no. 1, p. 162–178, https://doi.org/10.1130/GES02650.1.

Science Editor: David E. Fastovsky
Associate Editor: Xuan-Ce Wang

Received 15 February 2023
Revision received 6 June 2023
Accepted 8 October 2023

Published online 8 January 2024

Chronostratigraphy of Miocene strata in the Berkeley Hills (California Coast Ranges, USA) and the arrival of the San Andreas transform boundary

Stacey H. Gerasimov[1,2], Eben B. Hodgin[1,3], James L. Crowley[4], and Nicholas L. Swanson-Hysell[1]

[1]Department of Earth and Planetary Science, University of California, Berkeley, California 94720, USA
[2]Department of Earth and Planetary Sciences, Yale University, New Haven, Connecticut 06511, USA
[3]Department of Earth, Environmental and Planetary Sciences, Brown University, Providence, Rhode Island 02912, USA
[4]Department of Geosciences, Boise State University, Boise, Idaho 83725, USA

ABSTRACT

Miocene strata of the Claremont, Orinda, and Moraga formations of the Berkeley Hills (California Coast Ranges, USA) record sedimentation and volcanism during the passage of the Mendocino triple junction and early evolution of the San Andreas fault system. Detrital zircon laser ablation–inductively coupled plasma–mass spectrometry (LA-ICP-MS) age spectra indicate a change in sedimentary provenance between the marine Claremont formation (Monterey Group) and the terrestrial Orinda and Moraga Formations associated with uplift of Franciscan Complex lithologies. A sandstone from the Claremont formation produced a detrital zircon chemical abrasion–isotope dilution–thermal ionization mass spectrometry (CA-ID-TIMS) maximum depositional age of 13.298 ± 0.046 Ma, indicating younger Claremont deposition than previously interpreted. A trachydacite tuff clast within the uppermost Orinda Formation yielded a CA-ID-TIMS U-Pb zircon date of 10.094 ± 0.018 Ma, and a dacitic tuff within the Moraga Formation produced a CA-ID-TIMS U-Pb zircon date of 9.974 ± 0.014 Ma. These results indicate rapid progression from subsidence in which deep-water siliceous sediments of the Claremont formation were deposited to uplift that was followed by subsidence during deposition of terrestrial sediments of the Orinda Formation and subsequent eruption of the Moraga Formation volcanics. We associate the Orinda tuff clast and Moraga volcanics with slab-gap volcanism that followed the passage of the Mendocino triple junction. Given the necessary time lag between triple junction passage and the removal of the slab that led to this volcanism, subsidence associated with ca. 13 Ma Claremont sedimentation and subsequent Orinda to Moraga deposition can be attributed to basin formation along the newly arrived transform boundary.

INTRODUCTION

Prior to the current transform boundary tectonic regime, the California margin (USA) is widely interpreted to have been situated in an Andean-type setting where the Farallon plate was subducting under the North American plate (Dickinson, 1981). In this framework, convergent tectonism gave rise to Sierran arc volcanism, a forearc basin in which the sedimentary rocks of the Great Valley Group were deposited, and an offshore accretionary wedge that resulted in the formation of the Franciscan Complex (Dickinson, 1981; Irwin, 1990; Wakabayashi, 2015). Subduction of a ridge segment of the Farallon-Pacific plate boundary led to the initial establishment of the Mendocino and Rivera triple junctions ca. 27 Ma (Atwater, 1970; Atwater and Stock, 1998; Furlong and Schwartz, 2004). The Mendocino triple junction subsequently migrated northward, thereby progressively lengthening the transform boundary along and near the coast of California, while the Rivera triple junction migrated southward toward Mexico (Atwater, 1970). This development of the transform margin has shaped the geology of coastal California through transtensional subsidence and sediment accumulation, transpressional uplift and mountain building, and slab-gap volcanism that tracked behind the migrating triple junction.

Basin development associated with the transform margin resulted in significant accumulations of Neogene sedimentary rocks (Crowell, 1974; Blake et al., 1978). These basins variably and diachronously formed atop Paleogene sedimentary rocks, Mesozoic plutonic rocks, metamorphic Franciscan Complex lithologies, and sedimentary rocks of the Great Valley Group (Blake et al., 1978). Offshore basins that developed along the transform margin accumulated thick successions of pelagic and hemipelagic sediments including units that are broadly grouped as the Monterey Group (Barron, 1986; Behl, 1999). While lithofacies within the group are variable, the Monterey Group is typically characterized by diatomaceous and organic-rich shales (Behl, 1999). Basins that developed along the transform margin also resulted in nonmarine

Stacey H. Gerasimov https://orcid.org/0000-0003-0363-0721, Eben Blake Hodgin https://orcid.org/0000-0002-6569-5232, James Crowley https://orcid.org/0000-0001-5069-0773, Nicholas Swanson-Hysell https://orcid.org/0000-0003-3215-4648

depocenters with accumulations of terrestrial sedimentary rocks (Crowell, 1974; Graham et al., 1984). Changes in fault geometry and arrangement along the margin have resulted in many of these Neogene depocenters that previously were transtensional having now become uplifted within the California Coast Ranges due to transpression (Crowell, 1974).

The California Coast Ranges also preserve Neogene volcanics interpreted to have erupted as the result of slab-gap volcanism following the passage of the Mendocino triple junction (Zandt and Furlong, 1982; Fox et al., 1985). Slab-gap volcanism results from decompression melting of upwelling asthenosphere as it migrates into the space previously occupied by the Farallon plate (the northern remnant of which is referred to as the Gorda–Juan de Fuca plate; Furlong and Schwartz, 2004). Support for this mechanism for Coast Ranges volcanism comes from multiple lines of evidence including the younging of volcanics to the northwest tracking behind the passage of the triple junction where there no longer would be a subducting slab (Fox et al., 1985; Wagner et al., 2011). Volcanism is concentrated toward the northern end of the widening slab gap, leading to this northward younging trend with some younger out-of-sequence volcanics in the slab-gap region (Wakabayashi, 1999, and references therein). Geochemical data from Coast Ranges volcanics indicate a combination of melt generated from a depleted asthenosphere source with variable crustal assimilation consistent with a rise of asthenosphere into the slab-gap region (Johnson and O'Neil, 1984; Cole and Basu, 1995; Hammersley and DePaolo, 2006). Numerous geophysical data sets support the presence of a slab gap in the present-day region south of the Juan de Fuca plate boundary including heat-flow data (e.g., Lachenbruch and Sass, 1980), gravity data (e.g., Jachens and Griscom, 1983), and seismic velocities (e.g., Benz et al., 1992). Upwelling asthenosphere into the slab window has been imaged tomographically by teleseismic waves (e.g., Liu et al., 2012) and is spatially associated with the Clear Lake volcanic field, which has been active into the Holocene (most recent eruption ca. 10,000 yr B.P.; Donnelly-Nolan et al., 1981). Active-source seismic experiments have revealed the presence of partial melt below Lake Pillsbury in northern California, which is ~45 km north of the Clear Lake volcanic field and ~35 km to the south of the southern boundary of the Juan de Fuca plate (Levander et al., 1998). Levander et al. (1998) proposed that this location will be the next volcanic center within the slab gap. Both the active Clear Lake volcanic center and the proposed Lake Pillsbury locus of future magmatism are located in regions where there is active transtension along the transform margin (Levander et al., 1998).

This study is focused on the Miocene succession of the Berkeley Hills assemblage which is part of the East Bay block (bound by the Hayward fault to the west and the Calaveras fault to the east; Fig. 1). This assemblage records subsidence and uplift along the transform margin as well as slab-gap volcanism. Chronostratigraphic control in the Berkeley Hills Assemblage stratigraphy can place constraints on the arrival of the transform margin to the East Bay block and the resulting dynamic tectonism of associated basins.

GEOLOGIC BACKGROUND

Berkeley Hills Assemblage Overview

Our study focuses on Miocene strata of the Berkeley Hills assemblage of the East Bay block (defined by Jones and Curtis [1991] as subterrane I and Graymer [2000] as assemblage I). This assemblage is bound by the Hayward and Moraga faults to the west and east, respectively, and is undergoing active transpressional deformation (Fig. 1). The oldest unit in the Berkeley Hills assemblage is the Cretaceous Great Valley Group (undivided marine sandstone, siltstone, shale, and minor conglomerate; Graymer, 2000). The Great Valley Group is mapped to have faulted contacts with unnamed Paleogene sandstone and mudstone units with sparse chronostratigraphic constraints (Graymer, 2000; McDougall and Block, 2014). The Miocene Claremont formation (interbedded marine porcelanite and/or chert and shale with minor sandstone) has long been considered part of the Monterey Group (Lawson, 1914) and is variably grouped with the underlying marine shale and sandstone sometimes referred to as the Sobrante formation (mapped as unnamed glauconitic mudstone by Graymer [2000]). The contact between the Great Valley Group and the Claremont formation has been interpreted as an erosional unconformity to the south of the Berkeley Hills (Hill, 1979; Barron, 1989; Chetelat, 1995), but the contact between the Claremont formation and older units is interpreted as faulted throughout the region by Graymer (2000) consistent with the geologic mapping of Wagner (1978).

Monterey Group strata are unconformably overlain by the Contra Costa Group in the Berkeley Hills assemblage. The basal formation of the Contra Costa Group is the Orinda Formation (terrestrial mudstone, sandstone, and conglomerate), which is followed by the Moraga Formation (terrestrial basalt flows, tuffs, and interbedded fluvial sandstones and conglomerates), Siesta Formation (lacustrine claystone, siltstone, sandstone, tuffs, and limestone), and the Bald Peak Formation (terrestrial basalt flows). Each formation within the Contra Costa Group is deposited conformably over each other (Fig. 2), with the Bald Peak Formation being the uppermost exposed unit in the eroded core of the Siesta Valley syncline. While there are extensive exposures of both the upper Claremont formation of the Monterey Group and the lower Orinda Formation of the Contra Costa Group, the contact itself is poorly exposed. The contact has generally been depicted as an erosional unconformity (e.g., Graham et al., 1984). However, varying interpretations have been put forward. Page (1950) described the contact between the Claremont and Orinda formations to be conformable based on observations during tunnel construction through the East Bay Hills, although observations during more recent tunnel construction led to interpretations that the contact is faulted (Boyd et al., 2020). Wagner (1978) interpreted the contact as faulted based on observed slickensides at a contact exposure along Grizzly Peak Boulevard (Oakland, California) with associated shearing in the upper Claremont formation. Wagner (1978) also documented dikes present in the Orinda Formation that are not found to continue into the Claremont formation. A contrasting perspective was put forward

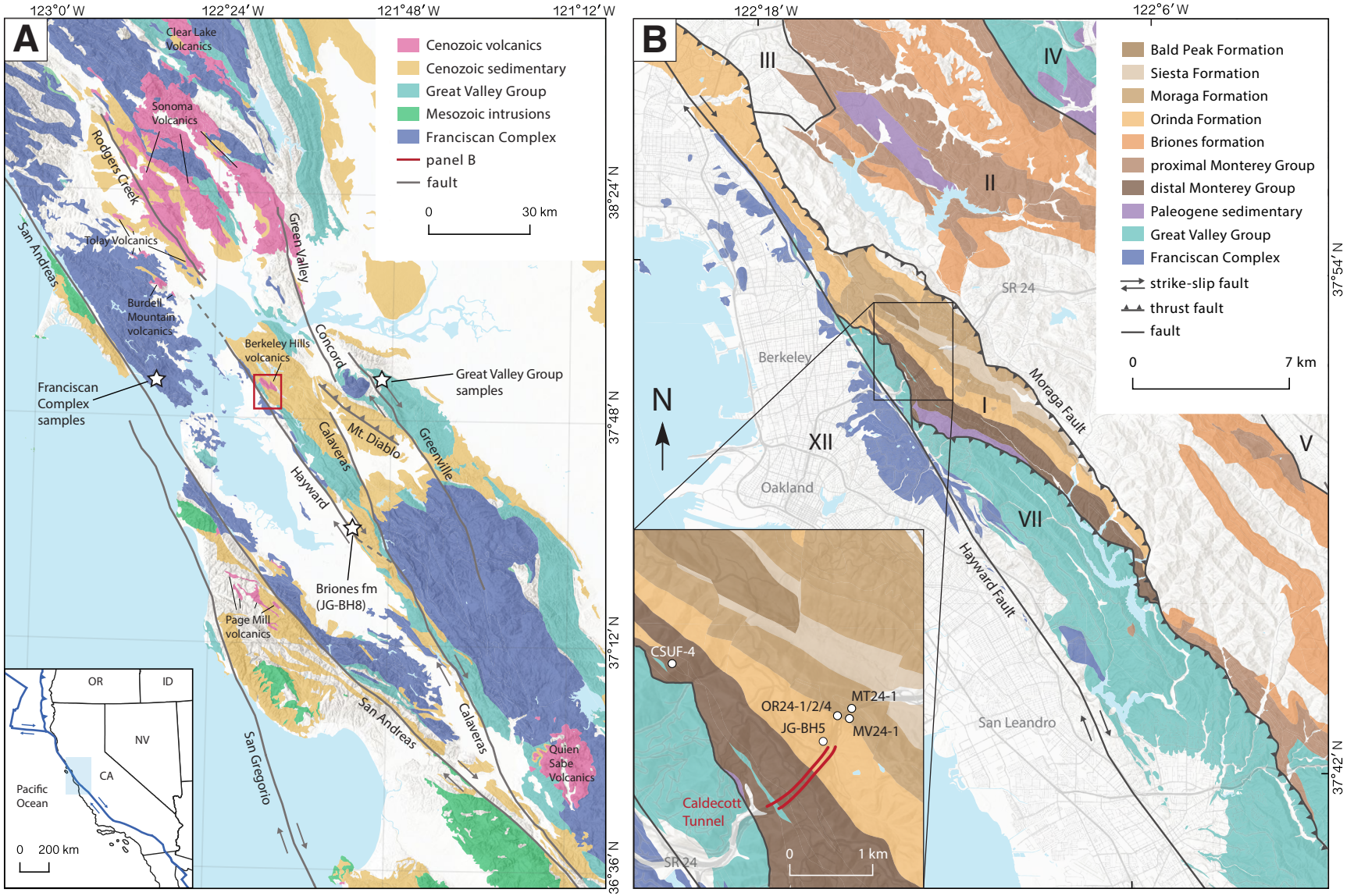

Figure 1. (A) Overview map of geology of the San Francisco Bay area (California, USA) highlighting major geologic groups (geologic data from Ludington et al., 2005). Locations of detrital zircon samples (white stars) from the Franciscan Complex (Bero et al., 2020), Great Valley Group (Sharman et al., 2015), and Briones formation (Gooley et al., 2021) discussed in the text are shown. (B) Geologic map of East Bay Hills study region (polygons from Graymer, 2000) with inset showing sample locations associated with this study as well as sample JG-BH5 from Gooley et al. (2021). Fault-bound assemblages are labeled with Roman numerals following the classification scheme of Graymer (2000). To simplify the map, we grouped unnamed Miocene units with the Sobrante(?) and Claremont formations in assemblage I as "distal Monterey Group" and the Sobrante, Claremont, Oursan, Tice, Hambre, and Rodeo formations in assemblages II, III, VII as "proximal Monterey Group" following the facies interpretations of Gooley et al. (2021) and map data of Graymer (2000). OR—Oregon; ID—Idaho; NV—Nevada; CA—California.

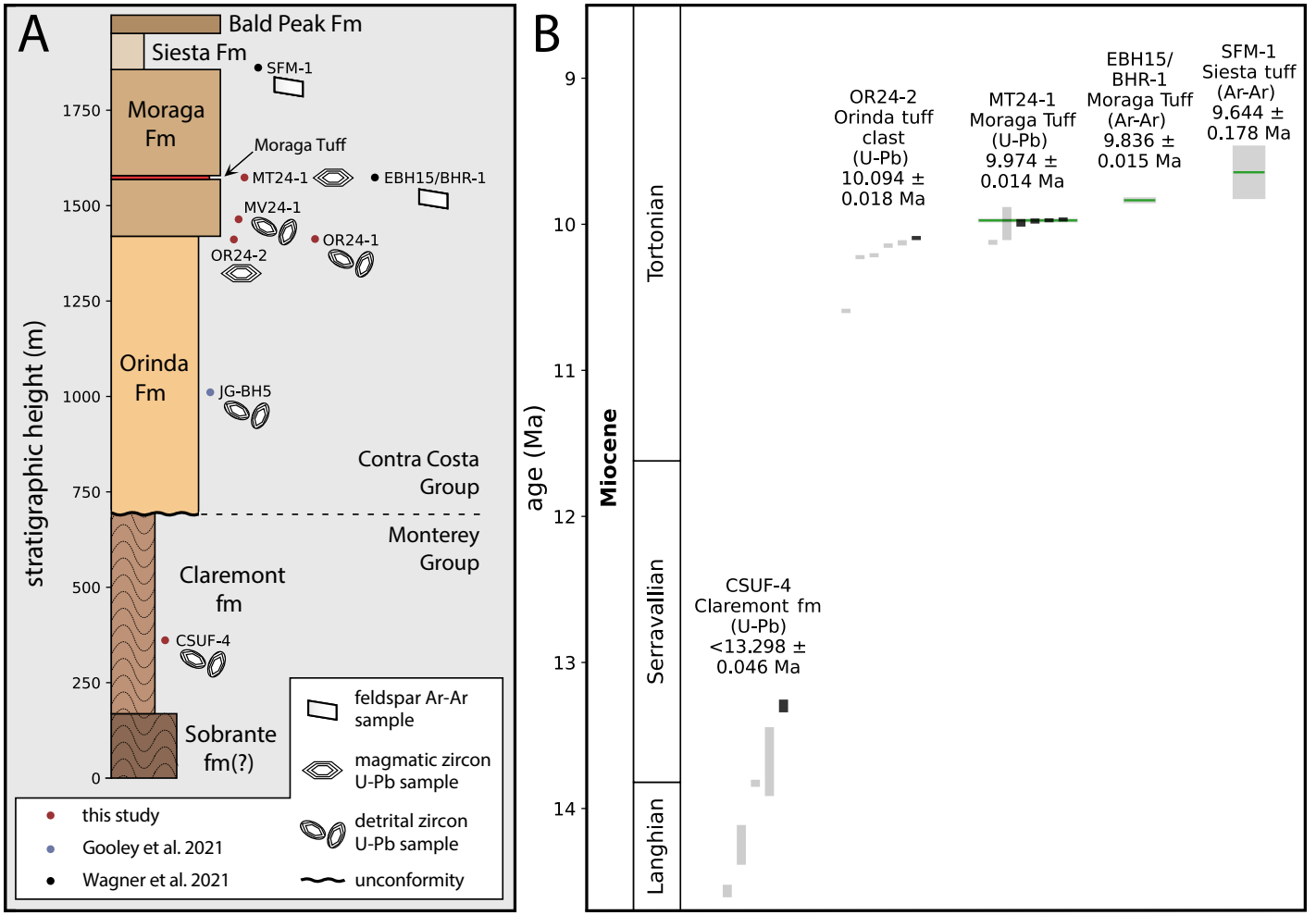

Figure 2. (A) Lithostratigraphic position of samples targeted in this study and previous studies. Note that the *y*-axis is in meters, not the chronostratigraphic time axis of panel B. Stratigraphic thicknesses of Contra Costa Group strata (Orinda, Moraga, Siesta, and Bald Peak) are well constrained because they are in a coherent dip panel but are more uncertain for the Monterey Group (Sobrante[?] and Claremont) due to structural complexity including folding and faulting. Contact between the groups is mapped as faulted by Graymer (2000) along Route 24, but could be interpreted as an erosional unconformity even if it is fault modified. (B) Date bar plot of individual U-Pb zircon dates determined through chemical abrasion–isotope dilution–thermal ionization mass spectrometry (CA-ID-TIMS) from detrital zircon grains of the Claremont formation (sample CSUF-4), zircon grains from a tuff clast within the upper Orinda Formation (sample OR24-2), and the prominent dacitic Moraga Tuff within the Moraga Formation (sample MT24-1). Black bars are those associated with the youngest concordant zircon or those included in the weighted mean shown as a green horizontal line. All U-Pb dates are presented with 2σ uncertainty that includes decay constant uncertainty. Also shown are Ar-Ar dates determined from the same Moraga Tuff (EBH15/BHR-1) and from a tuff within the Siesta Formation (SFM-1) from Wagner et al. (2021).

in Wagner et al. (2021) where a thin pebbly interval with Claremont chert clasts was described in the basal-most Orinda Formation (with such clasts absent throughout the rest of the formation in the Berkeley Hills assemblage), leading to an interpretation of an erosional unconformity. Claremont and other Monterey Group clasts appear in basal and upper beds of the Orinda Formation in distinct structural blocks from the Berkeley Hills assemblage within the southern East Bay Hills (Wagner et al., 2021). Graham et al. (1984) described the contact as a probable unconformity while noting that the contact is variably poorly exposed and structurally disrupted. Taken together, these observations are consistent with the contact being a variably fault-modified erosional unconformity.

Local lithological differences between neighboring assemblages and the Berkeley Hills assemblage are interpreted to be the result of fault juxtaposition in addition to lithofacies variability (Jones and Curtis, 1991; Graymer, 2000; Wagner et al., 2021). One notable difference between the Berkeley Hills and neighboring assemblages is the absence in the Berkeley Hills assemblage of the relatively proximal to paleoshoreline upper units of the Monterey Group: Oursan, Tice, Hambre, and Rodeo formations—interpreted to be time equivalents to the distal relative to paleoshoreline Claremont formation by Gooley et al. (2021). In this framework, the thin, meter-scale sandstone units of the Claremont formation could be interpreted as distal equivalents to thicker sandstone units mapped as the Oursan and Hambre formations along strike. One alternative interpretation is that the proximal units of the Monterey Group could have been erosionally removed prior to Orinda deposition. The presence of a preserved Miocene volcanic center, referred to as the Berkeley Hills volcanics (Moraga and Bald Peak formations), with intrusive and extrusive components is a largely unique aspect of the Berkeley Hills assemblage among the fault-bound assemblages of the East Bay region (Graymer, 2000). However, nearby volcanics in Union City that are interbedded with the Orinda Formation have interbedded flows with reported Ar-Ar dates of 10.84 ± 0.01 Ma and 10.46 ± 0.08 Ma, which is consistent with a northward-younging age progression (Fay and Fleck, 2014; Sullivan et al., 2021). Evidence of Miocene magmatic activity in other fault-bound assemblages in the region include tuffs within equivalents to the Contra Costa Group (Wagner et al., 2021) as well as ca. 7.8–7.5 Ma dacite intrusions east of Mount Diablo (Sullivan et al., 2021). Lavas interpreted to have been part of the Moraga Formation volcanics are also preserved on the west side of the Hayward fault, having been dextrally translated to the north of the modern-day San Francisco Bay and exposed in Sonoma County (the Tolay Volcanics in Fig. 1A; Fox et al., 1985; Wagner et al., 2011).

Monterey Group

Monterey Group strata throughout coastal California are characterized by diachronous, variably sediment-starved, organic-rich sedimentary rocks deposited in marine basins associated with the transform margin (Blake et al., 1978; Pisciotto and Garrison, 1981). A simplified stratigraphic framework for the Monterey Group is that it typically comprises three successive lithofacies: a lower calcareous facies of predominantly foraminiferal-coccolith shale, a middle transitional unit consisting of phosphatic shale, and an upper siliceous facies that includes diatomite (variably altered to porcelanite and chert) and diatomaceous shale (Pisciotto and Garrison, 1981). However, given that the group was deposited during subsidence at different times in different basins, significant variability is present (Pisciotto and Garrison, 1981). The Claremont formation is best described as the upper siliceous lithofacies: diatomite and diatomaceous shale that were later altered to chert and shale (Pisciotto and Garrison, 1981; Murray et al., 1992). Pisciotto and Garrison (1981) suggested that the transition from dominantly calcareous to dominantly siliceous sedimentation within the Monterey Group occurred ca. 13–12 Ma, which would be younger than the canonical age range for the Claremont formation (Jones and Curtis, 1991). Such siliceous sediments are associated with strong nutrient-rich upwelling that facilitated high productivity associated with diatom blooms and the associated deposition of diatomite when not diluted by terrestrial siliciclastic input (Flower and Kennett, 1993). Evaluating the hypothesis that such deposition was invigorated ca. 13–12 Ma necessitates enhanced chronostratigraphic control across the Monterey Group.

Broadly, the integration between strontium isotopic stratigraphy and biostratigraphy based on diatoms, calcareous nannofossils, and benthic foraminifera constrain Monterey Group deposition along the California margin to span from ca. 18 to 8 Ma (DePaolo and Finger, 1991). In the Berkeley Hills assemblage, Monterey Group deposition is broadly constrained to be sometime within the middle Miocene (Langhian to Serravallian Ages; <15.99 Ma; Raffi et al., 2020) based on 22 identified molluscan taxa from the sandstone unit below the Claremont formation, which is variably unnamed or referred to as the Sobrante formation (Powell et al., 2019). These same taxa have been used to interpret a depth of deposition of ~350–400 m (Powell et al., 2019). The Claremont formation contains sparse macrofossils, with the provisional identification of the bivalve *Lucinoma annulatum* suggestive, but not conclusive, of a middle to possible late Miocene age (Powell et al., 2019; where usage of "middle Miocene" implies the Langhian and Serravallian Ages and "late Miocene" the Tortonian and Messinian Ages). Microfossil biostratigraphic constraints for the Claremont formation come from six species of foraminifera identified by Kleinpell (1938) and interpreted to be from the Luisian provincial benthic stage (ca. 14.9–13.6 Ma; age range assigned to the stage from McDougall and Block, 2014) although these species range into the older Relizian stage (ca. 17.5–14.9 Ma; McDougall and Block, 2014) as well (Jones and Curtis, 1991). McDougall and Block (2014) reported most Claremont samples they investigated for micropaleontology as either being barren or containing species with long durations in the Miocene (*Fursenkoina californiensis* and *Siphogenerina* spp.) that provide little chronostratigraphic insight. Overall, the biostratigraphic constraints for the timing of Claremont formation deposition are sparse, which motivates the development of new radiometric dates in this study.

Contra Costa Group

The lowermost formation of the Contra Costa Group, the Orinda Formation, comprises nonmarine pebble to boulder conglomerates, conglomeratic sandstones, fine- to coarse-grained lithic sandstones, and mudstones (Estes et al., 1983; Graymer, 2000). At the California State Route 24 section (Fig. 1B), the Orinda Formation tends to coarsen upwards with thicker conglomerate beds toward the top of the formation (Wagner, 1978; Estes et al., 1983; Graham et al., 1984). The clasts of the conglomerate include very distinctive lithologies such as glaucophane schist that can be definitively considered to be derived from the Franciscan Complex (Creely et al., 1982). Clast counts (n = 585) in Graham et al. (1984) assign 65% of clasts to the Franciscan Complex and 33% of clasts to be from either the Franciscan Complex or the Great Valley Group, with the remainder being intraformational. Notably, there are rhyodacite tuff clasts within conglomerates in the upper part of the formation, one of which (a trachydacite) we sampled for U-Pb geochronology. The clast-supported conglomerates of the formation are variably imbricated, which enables determination that the currents within the fluvial channels that deposited the coarse-grained bedload flowed primarily from west to east. The conglomerate beds are channelized, fine upwards, and may be separated by meter-scale packages of mudstone (Graham et al., 1984). These observations led Graham et al. (1984) to propose that the Orinda Formation represents a fluvial system deposited on an alluvial plain where sediment was sourced from highlands to the west with Franciscan Complex bedrock. These alluvial plain deposits transition to shallow-marine deposits in sedimentary rocks interpreted to be coeval to the east, albeit ones in a distinct fault-bound assemblage (Graham et al., 1984; Buising and Walker, 1995). This interpretation is consistent with recent U-Pb detrital zircon maximum depositional ages of the contemporaneous Neroly and Briones formations of the San Pablo Group (Gooley et al., 2021). Terrestrial mammal fossils discovered within the Orinda Formation in the Berkeley Hills assemblage include horse and rodent fragments that have been assigned to the Clarendonian North American mammal stage (as reviewed in Poust, 2017), the age range of which has been interpreted to be from ca. 13.6 to 10.3 Ma (Alroy, 2000). In the lowermost Orinda Formation to the southeast of the Berkeley Hills assemblage (in the distinct assemblage II of Graymer, 2000), an Ar-Ar date of 11.544 ± 0.046 Ma on the Cull Canyon tuff constrains the timing of the onset of terrestrial deposition atop the Monterey Group (Wagner et al., 2021). Wagner et al. (2021) interpreted this constraint, as well as the vertebrate paleontology from the Orinda in the Berkeley Hills assemblage (their appendix B; Woodburne et al., 1981), to imply that the onset of Orinda Formation deposition in the Berkeley Hills assemblage is of similar age. There is the potential, however, that the onset of Orinda Formation deposition across these fault-bound assemblages is diachronous.

The uppermost siltstone and fine-grained sandstone of the Orinda Formation was baked as the lowermost basalt flow of the Moraga Formation flowed atop it. In the Berkeley Hills, a lower sequence of basalt flows with intervening sandstone and conglomerate is followed by a distinctive ~10-m-thick dacitic tuff (variably referred to as the Berkeley Hills tuff or the Moraga Tuff; Fig. 2). Stratigraphically atop this tuff are more basaltic lava flows and thicker interflow conglomerates. For decades, a number of unpublished K-Ar dates for the Moraga Formation (formerly referred to as the Grizzly Peak basalt) developed by Prof. Garniss Curtis (University of California, Berkeley) were commonly cited in the literature and constrained the timing of volcanism to have occurred between ca. 10.2 and 9.6 Ma (Curtis, 1989; Jones and Curtis, 1991; Graymer et al., 2002; Wagner et al., 2011). Subsequently, unpublished data from a conference abstract (Grimsich et al., 1996) developed Ar-Ar step heating age constraints for a Moraga basalt that placed the timing of volcanism to have begun by 9.99 ± 0.02 Ma (cited by Wakabayashi [1999], Graymer et al. [2002], and Wagner et al. [2021]). The first published radiometric age constraint for the Moraga Formation comes from Wagner et al. (2021), an Ar-Ar date from sanidine phenocrysts of the Moraga Tuff that was reported as 9.8356 ± 0.015 Ma (2σ). We targeted the Moraga Tuff for U-Pb zircon geochronology in this study. Within the lacustrine sedimentary rocks of the Siesta Formation overlying the Moraga Formation, a tuff was analyzed for Ar-Ar geochronology with a date of 9.644 ± 0.178 Ma (2σ) developed from plagioclase phenocrysts (Fig. 2; Wagner et al., 2021). These dates constrain the volcanics of the Moraga Formation to have erupted rapidly (Fig. 2).

METHODS

Three sandstone samples were collected for U-Pb detrital zircon geochronology, and two tuff samples (one clast and one in situ bed) were collected for high precision U-Pb zircon dating (Figs. 1 and 2). A sample of Claremont formation sandstone was collected as CSUF-4 from an outcrop along the side of the Upper Fire Trail in the Berkeley Hills (37.87055°N, 122.2319°W; Figs. 1 and 2). The remaining samples were collected from outcrops to the east of the Caldecott Tunnel along the northern side of Route 24—with the exception of a Moraga Formation interflow sandstone sample which was collected from the southern side of the highway (Fig. 1). A sample of Orinda Formation sandstone (OR24-1) was collected 7.2 m from the top of the formation (37.86527°N, 122.2089°W; Figs. 1 and 2). A 19-cm-diameter subangular cobble of trachydacite tuff within an Orinda Formation conglomerate was collected as OR24-2 at the same locality 8.4 m from the top of the formation (37.86527°N, 122.2089°W; Figs. 1 and 2). A sample of Moraga Formation interflow sandstone was collected between basaltic lava flows as MV24-1 (37.86500°N, 122.20722°W; Figs. 1 and 2). The Moraga Tuff was sampled as MT24-1 (37.86611°N, 122.2069°W; Figs. 1 and 2).

Following crushing of the samples, zircon were separated from the samples through hand panning, magnetic separation, and heavy liquids. At Boise State University (Boise, Idaho, USA), U-Pb dates on zircon were determined for all samples through laser ablation–inductively coupled plasma–mass spectrometry (LA-ICP-MS) with two goals: (1) to conduct a provenance study on detrital zircon from sandstone samples and (2) to screen both tuff and sandstone samples for the youngest

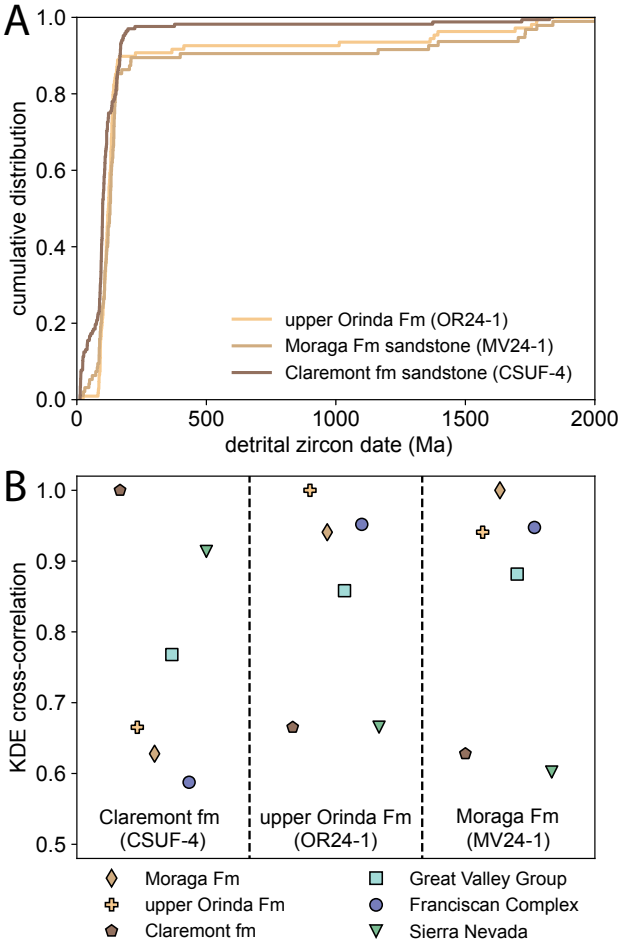

Figure 3. (A) Cumulative distribution plots of detrital zircon dates determined through laser ablation–inductively coupled plasma–mass spectrometry (LA-ICP-MS) from this study, highlighting the similarity between the distribution of detrital zircon dates from sandstone of the upper Orinda Formation and that of interflow sandstone deposited between basaltic lava flows in the Moraga Formation. Claremont formation sandstone has a distinct distribution characterized by more Cenozoic grains (including Miocene grains that were subsequently targeted for chemical abrasion–isotope dilution–thermal ionization mass spectrometry [CA-ID-TIMS]; Fig. 2) and a relative lack of Paleozoic and Precambrian grains. (B) Samples in A are compared to each other and to Franciscan Complex and Great Valley Group detrital zircon data and Sierra Nevada magmatic ages (see ages and citations in Fig. 4) through kernel density estimate (KDE) cross-correlation values with an arbitrary *x*-axis that spreads out the points. As in a cross-correlation matrix, the values are shown fully correlated with themselves. Claremont formation exhibits a high KDE cross-correlation with the Sierra Nevada ages, while the Moraga Formation and Orinda Formation sandstones have a high correlation compared with each other and with detrital zircon from sandstones of the Franciscan Complex.

zircon grains to target for higher precision chemical abrasion–isotope dilution–thermal ionization mass spectrometry (CA-ID-TIMS; Fig. 3). Methods for both LA-ICP-MS and CA-ID-TIMS analyses are as described in Hodgin et al. (2022). CA-ID-TIMS dates were determined for both of the tuff samples (OR24-2 and MT24-1; Fig. 2). The youngest detrital zircon identified by LA-ICP-MS from the Claremont formation sandstone were also dated via CA-ID-TIMS so that the maximum depositional age could be constrained more accurately and precisely (Fig. 2).

The tuff clast (OR24-2) and a sample of Moraga Formation basalt (OR24-4; 37.86527°N, 122.2089°W) were also sampled for whole-rock geochemistry (see Supplemental Material[1]). Samples were pulverized using a ceramic grinding container at the University of California, Berkeley. Major and trace element abundances were measured by X-ray fluorescence (XRF) on lithium tetraborate ($Li_2B_4O_7$) fusion disks at Franklin and Marshall College (Lancaster, Pennsylvania, USA), following standard methods as in Mertzman (2000).

RESULTS

LA-ICP-MS

LA-ICP-MS U-Pb detrital zircon dates are summarized in Figures 3 and 4. These data include 169 concordant analyses from the Claremont Formation sandstone (CSUF-4), 109 concordant analyses from the upper Orinda Formation sandstone (OR24-1), and 96 concordant analyses from the Moraga Formation interflow sandstone (MV24-1). In Figure 3A, the empirical cumulative distributions of the dates from these samples are shown together. These cumulative distributions highlight the similarity between the Orinda and Moraga Formation sandstones and the contrast with the Claremont formation sandstone. The Claremont formation data set contains Cenozoic dates (18% of grains) with a Miocene peak that is absent from the Orinda Formation sandstone and smaller in the Moraga Formation interflow sandstone (6% of grains). The Orinda and Moraga Formation sandstone samples have a significant proportion of pre-Mesozoic grains (10% and 11%, respectively), while only 3% of the Claremont formation dates pre-date the Mesozoic (Fig. 3). The relative similarity between the provenance of these samples can be assessed using kernel density estimate (KDE) cross-correlation (Saylor and Sundell, 2016), which is visualized in Figure 3B. The Orinda Formation sandstone and Moraga Formation interflow sandstone dates have a KDE cross-correlation of 0.94 with each other compared to a KDE cross-correlation of 0.66 and 0.62, respectively, with the Claremont formation sandstone (Fig. 3B).

We compare detrital zircon spectra for these samples to the age distributions of candidate provenance lithologies, including a compilation of

[1]Supplemental Material. Table of U-Pb geochronology data (Table S1: LA-ICP-MS data), table of whole-rock geochemistry data (Table S2: XRF data), measured stratigraphic sections (Figs. S1–S4), an annotated field photo of the upper Orinda Formation samples (Fig. S5), and a total alkali–silica plot (Fig. S6). Please visit https://doi.org/10.1130/GEOS.S.24596220 to access the supplemental material, and contact editing@geosociety.org with any questions.

Sierra batholith magmatic ages (Chapman et al., 2012), detrital zircon dates from sandstone of the Great Valley Group in the Mount Diablo area (Sharman et al., 2015), and detrital zircon dates from sandstone of the Franciscan Complex in the Mount Tamalpais area (Bero et al., 2020). The peaks of the detrital zircon age spectra of the Claremont formation sandstone match the ca. 100 Ma and ca. 165 Ma peaks in ages from the Sierra batholith (Fig. 4), resulting in a high KDE cross-correlation value of 0.91 between the data sets (Fig. 3). In contrast, the Orinda Formation sandstone and Moraga Formation interflow sandstone data sets have a broader Mesozoic population as well as pre-Mesozoic grains that are very similar to the distribution of detrital zircon in the Franciscan Complex compilation, leading to KDE cross-correlation values of 0.95 for both samples with the Franciscan Complex data (Fig. 3). This finding of a dominantly Franciscan Complex provenance is consistent with the Franciscan-derived clast composition of the conglomerates within the Orinda Formation. Taken together, these data document a significant shift in the provenance of detritus delivered to the Claremont formation versus that delivered to the terrestrial sedimentary units of the Contra Costa Group. We note that the Franciscan Complex itself contains abundant Mesozoic zircon likely derived from Sierran arc volcanic sources, which were then recycled from the uplifted Franciscan Complex into the Contra Costa Group sediments. This interpretation is supported by U/Yb versus Nb/Yb of Sierran-aged detrital zircon in Franciscan-derived terrestrial sediments of the Contra Costa Group that are consistent with a continental arc source (Fig. 5). The Franciscan Complex samples have dates from the ca. 140–120 Ma magmatic lull in the Sierra Nevada and also contain significant pre-Mesozoic grains including Proterozoic zircon. While differences in the age spectra appear subtle, they enable a fingerprint (Fig. 3) that is consistent with more routing of material from the continental interior to the margin at the time of Cretaceous Franciscan Complex deposition than at the time of Miocene Claremont formation deposition. It has also been shown that Great Valley Group forearc strata, of similar age to sedimentary rocks of the Franciscan Complex, also contain significant populations from the Sierra Nevada magmatic lull (Surpless et al., 2019). It is therefore likely that the Great Valley Group was not delivering detritus to the basin at the time of Claremont formation deposition—likely due to the Great Valley Group remaining buried. In contrast, KDE cross-correlation values between the Orinda Formation sandstone and Moraga Formation interflow sandstone spectra and that of the Great Valley Group are higher than the cross-correlation value between the Claremont and Great Valley Group (0.86 and 0.88, respectively, versus 0.77), which could be consistent with it as a source. These values are not as high as those of the Franciscan Complex dates, but the similarity between Franciscan Complex and Great Valley Group detrital zircon spectra make the sources difficult to distinguish (Fig. 4). However, the dominance of Franciscan Complex lithologies as clasts in the Orinda Formation favor an interpretation that the Franciscan Complex is the major zircon provenance source as well.

Of the youngest detrital zircon grains dated in our provenance study, the majority are found in the Claremont formation sandstone sample, which yielded six LA-ICP-MS dates between 13 and 12 Ma (Fig. 4). Five of these zircon grains were selected for more accurate and precise CA-ID-TIMS analysis in order to develop a high-precision maximum depositional age. The Orinda Formation sandstone sample lacked any Miocene-aged zircon, while the Moraga Formation interflow sandstone only had one grain at ca. 12 Ma (Fig. 4). The paucity of Miocene-aged zircon grains in the interflow sandstone is striking given that the sediments were deposited within a Miocene-age volcanic field. The lack of Miocene zircon grains in this interflow sandstone can be explained through the associated fluvial system having developed atop zircon-poor basaltic lava flows and the depositional system being swamped with detritus sourced from the Franciscan Complex.

CA-ID-TIMS

We conducted CA-ID-TIMS analyses on the youngest zircon identified through LA-ICP-MS from the Claremont formation sample (CSUF-4), zircon from the trachydacite tuff clast collected within the Orinda Formation conglomerate (OR24-2), and zircon from the dacitic Moraga Tuff (MT24-1). The dates from the Claremont formation sandstone and Orinda Formation tuff clast samples provide maximum depositional ages, while the data from the Moraga Tuff provide crystallization ages of zircon within the associated magmatic system. $^{206}Pb/^{238}U$ CA-ID-TIMS dates for the Claremont formation zircon (CSUF-4) range from ca. 14.6 to 13.3 Ma. We interpret the youngest $^{206}Pb/^{238}U$ date of 13.298 ± 0.044/0.044/0.046 Ma as giving the maximum depositional age. Results are given in the ± *X*/*Y*/*Z* format (where *X* is the analytical error, *Y* includes additional tracer calibration error, and *Z* incorporates the U decay constant uncertainties of Jaffey et al., 1971, and Hiess et al., 2012) and are reported with 2σ uncertainty (Table 1).

For the trachydacite tuff clast within the Orinda Formation conglomerate (OR24-2), individual zircon dates range from ca. 10.59 ± 0.02 to ca. 10.09 ± 0.01 Ma (Table 1). We interpret these data to indicate that there was a range of zircon crystallization times within the magmatic system from which the tuff erupted. We interpret the youngest $^{206}Pb/^{238}U$ date of 10.094 ± 0.014/0.014/0.018 Ma as the best representation of the eruptive age for the tuff and therefore as a maximum depositional age for the upper Orinda Formation (Fig. 2). Given the angularity and relative fragility of the tuff clast relative to other clasts of the formation, we interpret it not to be far traveled. This date is likely of a very similar age to the depositional age, particularly in the context of dates from the overlying Moraga Formation (Fig. 2).

For the Moraga Tuff (MT24-1), a weighted mean $^{206}Pb/^{238}U$ date of 9.974 ± 0.008/0.009/0.014 Ma (n = 4; mean square weighted deviation [MSWD] = 0.93) was calculated from four individual zircon dates (Fig. 2; Table 1). This weighted mean excludes: one imprecise date associated with a low ratio of radiogenic to common lead (analysis z3; LA-ICP-MS spot M64), one high-precision analysis of 10.124 ± 0.017 Ma (analysis z7; LA-ICP-MS spot L17) that is likely associated with earlier crystallization of zircon within the magmatic system, and one date of 133.07 ± 0.096 Ma from a zircon (analysis z5) not

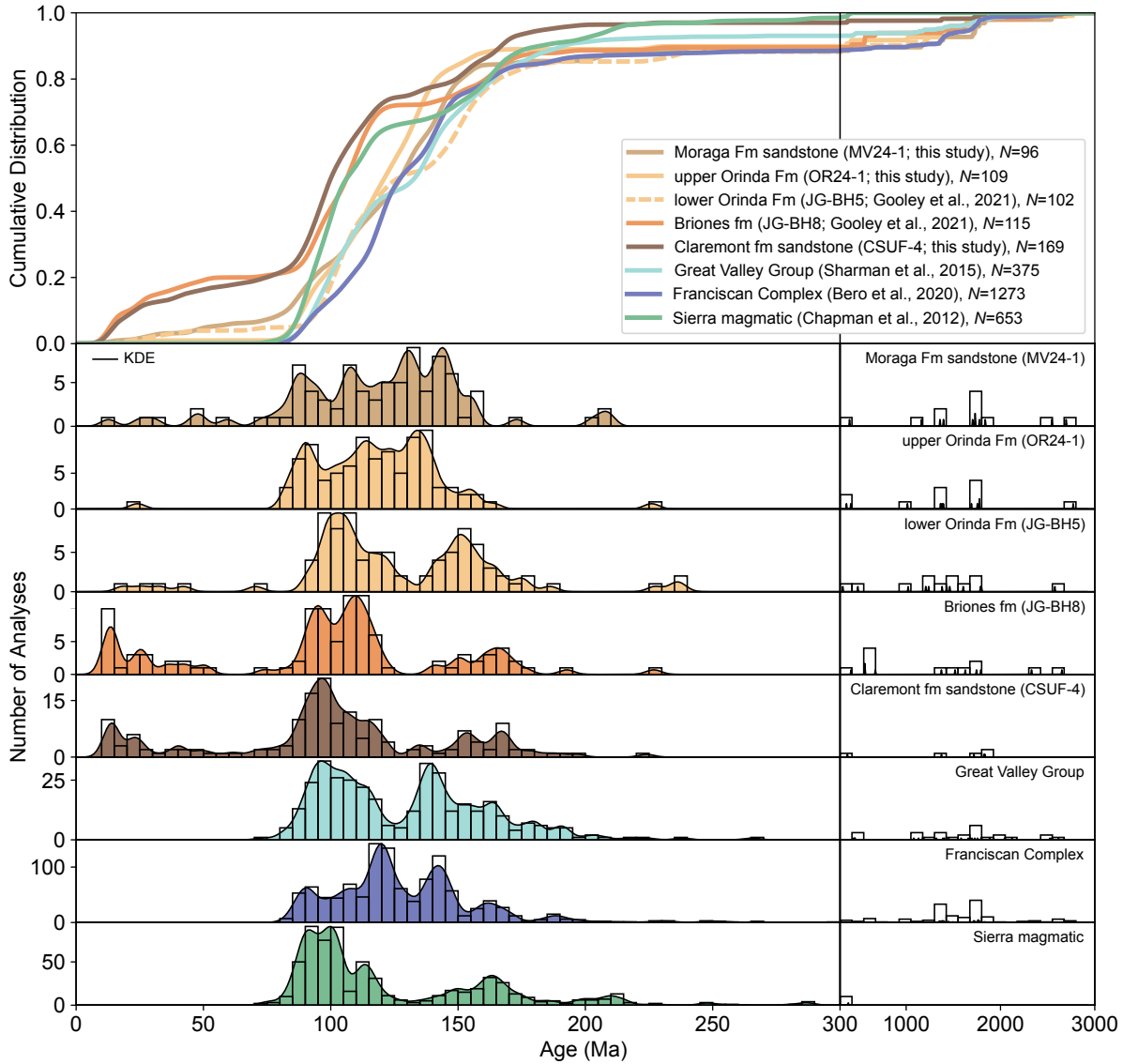

Figure 4. U-Pb detrital zircon data from this study and previous studies shown as cumulative distribution estimates in the upper panel, and kernel density estimates (KDE) plotted atop age distribution histograms in the lower panels (plots made using detritalPy; Sharman et al., 2018). Note change in horizontal scale at 300 Ma. Sierra batholith crystallization dates come from the compilation of Chapman et al. (2012); Franciscan Complex detrital zircon data come from lithic and feldspathic sandstone of the Mount Tamalpais area (Fig. 1; Bero et al., 2020); Great Valley Group detrital zircon sandstone samples come from the Mount Diablo area (Fig 1; Sharman et al., 2015); Briones sample comes from sandstone in Morrison Canyon in Fremont, California, south of the Berkeley Hills assemblage (Fig. 1; Gooley et al., 2021); the lower Orinda sample comes from a sandstone outcrop near the eastern entrance of the Caldecott Tunnel (Gooley et al., 2021) in the same stratigraphic panel as the samples of this study (Figs. 1 and 2). Detrital zircon from this study are from samples of sandstone that appear along the side of Route 24 (OR24-1, MV24-1) and the Upper Fire Trail in the Berkeley Hills (CSUF-4).

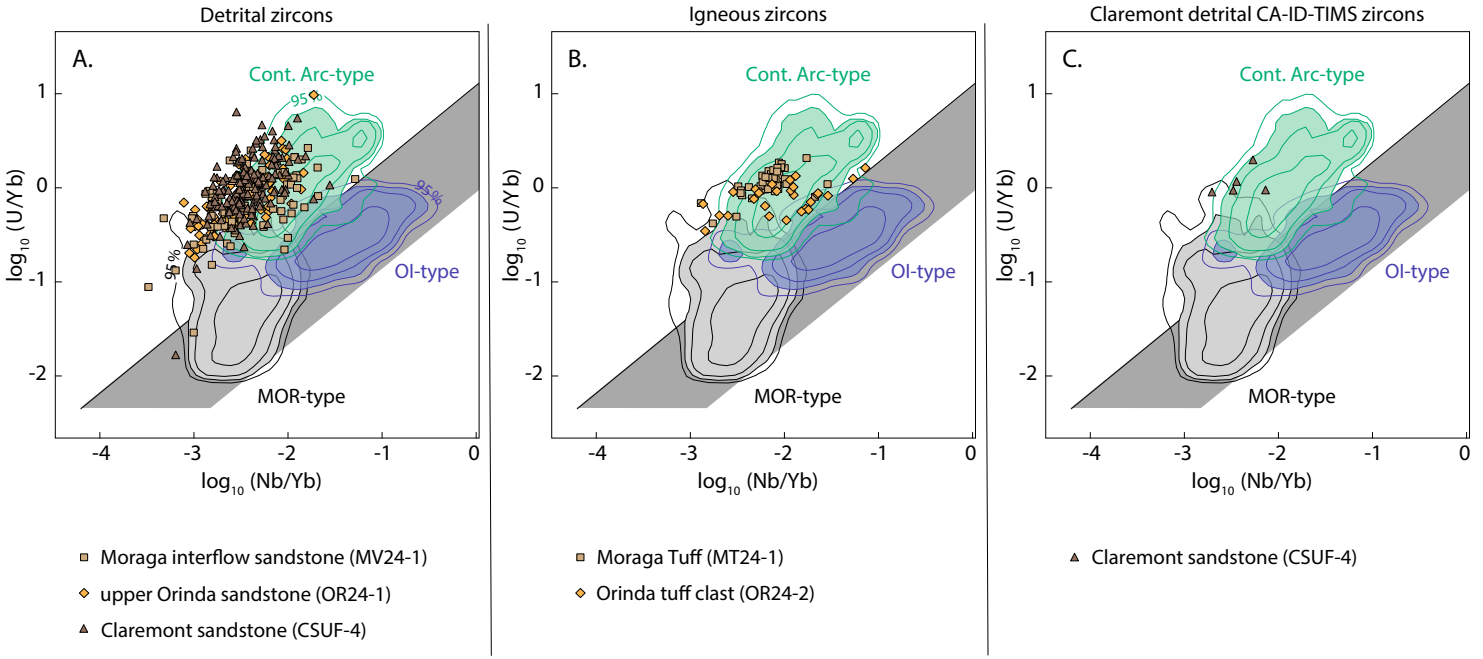

Figure 5. Zircon trace element data from this study plotted on Nb/Yb versus U/Yb cross-plots atop density distributions of compiled data from distinct tectono-magmatic settings. Shaded fields are kernel density distributions for compiled data sets of mid-ocean-ridge (MOR-type), ocean-island (OI-type), and continental-arc (Cont. Arc-type) zircon from Grimes et al. (2015). Contours represent the proportion of points inside 50%, 80%, 90%, and 95% levels. Diagonal shaded bands represent the "mantle-zircon array" defined in Grimes et al. (2015). (A) Trace elements of detrital zircon from sandstone samples within the Claremont, Orinda, and Moraga formations. (B) Trace elements of zircon from tuff samples within the Orinda and Moraga formations. (C) Trace elements of Miocene-age zircon selected for chemical abrasion–isotope dilution–thermal ionization mass spectrometry (CA-ID-TIMS) analysis from the Claremont sandstone sample.

pre-screened by LA-ICP-MS that likely is a grain inherited from host rock or sediment during eruption and emplacement of the tuff. This weighted mean $^{206}Pb/^{238}U$ date of 9.974 ± 0.014 Ma for the Moraga Tuff is older than the 9.836 ± 0.015 Ma Ar-Ar date (Wagner et al., 2021) from sanidine phenocrysts of the same tuff (Fig. 2). We interpret the older zircon crystallization date to be associated with melt generation and crystallization occurring ~140 k.y. prior to eruption of the tuff recorded by the Ar-Ar date.

DISCUSSION

We interpret the subsidence, uplift, and volcanism recorded within the Miocene strata of the Berkeley Hills assemblage to be associated with the arrival and progressive development of the transform margin. Monterey Group deposition within the Berkeley Hills assemblage has been interpreted to have occurred within a forearc basin prior to the arrival of the transform margin to the East Bay block (Graham et al., 1984; Gooley et al., 2021). While previous chronostratigraphic control from biostratigraphy broadly placed deposition in the middle Miocene (Kleinpell, 1938; Powell et al., 2019), our high-precision maximum depositional age from within the Claremont formation of 13.298 ± 0.046 Ma adds new constraints. This date constrains Monterey Group deposition in the region as being temporally close to the subsequent deposition and magmatic activity of the Contra Costa Group. As a result, it is likely that the Claremont formation was deposited in a basin that developed due to transtension associated with the arrival of the Mendocino triple junction to the region where the Berkeley Hills assemblage was deposited. We propose that basin formation related to transtension initiated at the base of the Monterey Group, with the initial pulse of subsidence rapidly leading to deposition in a relatively deep basin, as is typical of strike-slip basins (Christie-Blick and Biddle, 1985; Xie and Heller, 2009). A tectonic setting along the transform margin is typical of basins in which the Monterey Group was deposited (Blake et al., 1978; Behl, 1999).

Along the California margin, passage of the triple junction and arrival of the transform margin

TABLE 1. U-Pb CA-ID-TIMS DATA

		Compositional parameters					Radiogenic isotope ratios									Isotopic dates (Ma)						
Sample and analysis no.	LA-ICP-MS spot no.	Th/U	$^{206}Pb^*$ ($\times 10^{-13}$ mol)	$^{206}Pb^*$ (mol%)	Pb^*/Pb_c	Pb_c (pg)	$^{206}Pb/^{204}Pb$	$^{208}Pb/^{206}Pb$	$^{207}Pb/^{206}Pb$	Error (%)	$^{207}Pb/^{235}U$	Error (%)	$^{206}Pb/^{238}U$	Error (%)	Corr. coef.	$^{207}Pb/^{206}Pb$	± Error (analytical)	$^{207}Pb/^{235}U$	± Error (analytical)	$^{206}Pb/^{238}U$	± Error (analytical)	± Error (analytical + tracer + decay constant)
(a)		(b)	(c)	(c)	(c)	(c)	(d)	(e)	(e)	(f)	(e)	(f)	(e)	(f)		(g)	(f)	(g)	(f)	(g)	(f)	(f)
MT24-1																						
z1	**L9**	**0.464**	**0.219822**	**0.95198**	**5.900**	**0.92**	**375.7**	**0.150**	**0.0465615**	**1.21919**	**0.0099399**	**1.320590**	**0.001549**	**0.1753**	**0.7564**	**25.71**	**29.13**	**10.04**	**0.13**	**9.978**	**0.017**	**0.021**
z3	M64	0.490	0.052041	0.66589	0.599	2.17	54.00	0.159	0.0502606	12.7865	0.0107482	13.50995	0.001552	1.1355	0.6597	206.02	295.52	10.86	1.46	9.995	0.113	0.114
z5	–	0.482	1.009658	0.99713	103.8	0.24	6284	0.154	0.0486930	0.17840	0.1399612	0.227349	0.020856	0.0727	0.7631	132.02	4.19	133.01	0.28	133.065	0.096	0.176
z6	**L12**	**0.606**	**0.326420**	**0.98029**	**15.38**	**0.54**	**915.5**	**0.196**	**0.0466800**	**0.54095**	**0.0099546**	**0.600522**	**0.001547**	**0.1401**	**0.7114**	**31.81**	**12.91**	**10.06**	**0.06**	**9.967**	**0.014**	**0.018**
z7	L17	0.454	0.099752	0.96127	7.365	0.33	465.8	0.147	0.0467278	1.33619	0.0101214	1.430914	0.001572	0.1677	0.7500	34.26	31.88	10.23	0.15	10.124	0.017	0.020
z8	**L22**	**0.429**	**0.386358**	**0.98413**	**18.28**	**0.52**	**1137**	**0.139**	**0.0466581**	**0.42633**	**0.0099554**	**0.480959**	**0.001548**	**0.1371**	**0.7010**	**30.69**	**10.18**	**10.06**	**0.05**	**9.973**	**0.014**	**0.018**
z9	**M42**	**0.493**	**0.046481**	**0.92232**	**3.560**	**0.32**	**232.3**	**0.160**	**0.0463924**	**4.13611**	**0.0099163**	**4.259569**	**0.001551**	**0.2568**	**0.5461**	**16.98**	**98.98**	**10.02**	**0.43**	**9.990**	**0.026**	**0.028**
																Weighted mean $^{206}Pb/^{238}U$ date = 9.974 ± 0.008/0.009/0.014 Ma (2σ); MSWD = 0.93 (n = 4)						
OR24-2																						
z1	**L71, L73**	**0.437**	**0.493356**	**0.98067**	**14.98**	**0.81**	**933.4**	**0.141**	**0.0464719**	**0.52232**	**0.0100361**	**0.578738**	**0.001567**	**0.1405**	**0.6681**	**21.10**	**12.49**	**10.14**	**0.06**	**10.094**	**0.014**	**0.018**
z2	L74	0.572	0.890203	0.99166	36.43	0.62	2164	0.185	0.0465044	0.24335	0.0101744	0.296663	0.001587	0.1410	0.6768	22.77	5.82	10.28	0.03	10.225	0.014	0.018
z3	L75	0.663	0.425146	0.98347	18.66	0.59	1092	0.215	0.0460666	0.51911	0.0100656	0.574584	0.001585	0.1399	0.6561	0.02	12.46	10.17	0.06	10.212	0.014	0.018
z4	L85	0.386	0.073598	0.97011	9.453	0.19	603.7	0.125	0.0466813	1.88458	0.0101144	1.981272	0.001572	0.1760	0.7059	31.88	44.98	10.22	0.20	10.127	0.018	0.021
z5	M53	0.598	0.313436	0.97665	12.92	0.62	772.8	0.194	0.0486134	0.62127	0.0110186	0.685089	0.001645	0.1399	0.7043	128.17	14.57	11.13	0.08	10.593	0.015	0.019
z6	M51	0.414	0.209519	0.97319	10.65	0.48	672.9	0.134	0.0465762	0.84551	0.0101107	0.918243	0.001575	0.1490	0.7254	26.47	20.20	10.21	0.09	10.146	0.015	0.019
																Youngest concordant $^{206}Pb/^{238}U$ date = 10.094 ± 0.014/0.014/0.018 Ma (2σ) (n = 1)						
CSUF-4																						
z1	**M316**	**0.504**	**0.030494**	**0.92097**	**3.506**	**0.22**	**228.3**	**0.163**	**0.0472581**	**7.86538**	**0.0134491**	**7.986562**	**0.002065**	**0.3289**	**0.3951**	**61.22**	**186.86**	**13.56**	**1.08**	**13.298**	**0.044**	**0.046**
z3	M340	0.457	0.024775	0.91051	3.023	0.20	201.6	0.147	0.0476074	12.6472	0.0148408	12.71374	0.002262	0.2952	0.2424	78.74	299.56	14.96	1.89	14.565	0.043	0.046
z4	M377	0.609	0.062685	0.95194	6.123	0.26	375.4	0.200	0.0463594	2.14721	0.0137192	2.244264	0.002147	0.1764	0.6328	15.27	51.46	13.84	0.31	13.827	0.024	0.029
z5	M383	0.941	0.005425	0.58302	0.475	0.32	43.27	0.300	0.0613000	205.589	0.0179455	205.6956	0.002124	1.7265	0.0656	648.81	4405.12	18.06	36.82	13.679	0.236	0.236
z6	S453	0.487	0.017926	0.70632	0.719	0.62	61.44	0.157	0.0457416	14.1197	0.0139497	14.64869	0.002213	0.9575	0.5737	–17.07	340.49	14.07	2.05	14.249	0.136	0.137
																Youngest concordant $^{206}Pb/^{238}U$ date = 13.298 ± 0.044/0.044/0.046 Ma (2σ) (n = 1)						

(a) z1, z2, etc. are labels for single zircon grains annealed and chemically abraded after Mattinson (2005); bold text indicates youngest concordant date or dates used in weight mean calculation.
(b) Model Th/U ratio iteratively calculated from the radiogenic $^{208}Pb/^{206}Pb$ ratio and $^{206}Pb/^{238}U$ age.
(c) Pb* and Pb_c represent radiogenic and common Pb, respectively; $^{206}Pb^*$ (mol%) is with respect to radiogenic, blank, and initial common Pb.
(d) Measured ratio corrected for spike and fractionation only. Fractionation is estimated at 0.18 ± 0.03 %/atomic mass unit for Daly analyses, based on analysis of reference materials NBS-981 and NBS-982.
(e) Corrected for fractionation, spike, and common Pb; as much as 1 pg of common Pb was assumed to be procedural blank: $^{206}Pb/^{204}Pb$ = 18.042% ± 0.61%; $^{207}Pb/^{204}Pb$ = 15.537% ± 0.52%; $^{208}Pb/^{204}Pb$ = 37.686% ± 0.63% (all uncertainties 1σ). Excess over blank was assigned to initial common Pb, using the Stacey and Kramers (1975) two-stage Pb isotope evolution model at the nominal sample age.
(f) Errors are 2σ, propagated using the algorithms of Schmitz and Schoene (2007); for corr. coef (correlation coefficient) calculations see Schmitz and Schoene (2007).
(g) Calculations are based on the decay constants of Jaffey et al. (1971) and Hiess et al. (2012). $^{206}Pb/^{238}U$ and $^{207}Pb/^{206}Pb$ ages are corrected for initial disequilibrium in $^{230}Th/^{238}U$ using Th/U [magma] = 3.
Notes: CA-ID-TIMS and LA-ICP-MS stand for chemical abrasion-isotope dilution-thermal ionization mass spectrometry and laser ablation-inductively coupled plasma-mass spectrometry, respectively; dash is the sample that was not pre-screened by LA-ICP-MS. MSWD—mean square weighted deviation.

led to alternating intervals of subsidence and uplift due to varying fault geometry with time (Fig. 6). Changes in fault geometry through time along transform margins results in strike-slip basins being the shortest-lived type of sedimentary basin (Woodcock, 2004). Such repeated cycles of subsidence and uplift associated with strike-slip systems, also referred to as porpoising (Nilsen and Sylvester, 1999) or yo-yo tectonics (Umhoefer et al., 2007), are processes that have been documented to take place on the order of less than a million years (e.g., Hengesh and Wakabayashi, 1995) to millions of years (e.g., Idleman et al., 2014). Such dynamic tectonic episodes are recorded in the Berkeley Hills stratigraphy as illustrated schematically in Figure 6.

The switch from hemipelagic marine deposition of the Claremont formation to terrestrial deposition of the Orinda Formation required a significant change in relative sea level (of at least 350 m; Powell et al., 2019). Fluctuations in global eustatic sea level likely ranged on the order of tens of meters during deposition of the Claremont and Orinda formations (Miller et al., 2020). The rapid and large change in relative sea level supports the interpretation that tectonic uplift of Monterey Group strata occurred and was followed by renewed subsidence leading to deposition of Contra Costa Group strata. Orinda Formation deposition initiated prior to 10.094 ± 0.018 Ma (based on the interpretation that the uppermost Orinda Formation tuff clast erupted syn-depositionally; Fig. 2). This timing may be consistent with the ca. 11.5 Ma age assigned to the base of the >500 m of Orinda Formation strata in the Berkeley Hills assemblage based on correlation to the southeast (Wagner et al., 2021). Given the Claremont formation maximum depositional age of 13.298 ± 0.046 Ma, the chronostratigraphy requires that the change from subsidence to uplift to renewed subsidence would have been geologically rapid. The major change in provenance associated with this renewed deposition required uplift of Franciscan Complex crustal blocks to the west which is reflected in the lithology of Orinda Formation clasts, which paleocurrent data indicate were transported from west to east (Graham et al., 1984), as well as in the detrital zircon provenance (Figs. 3 and 6). This change in provenance is

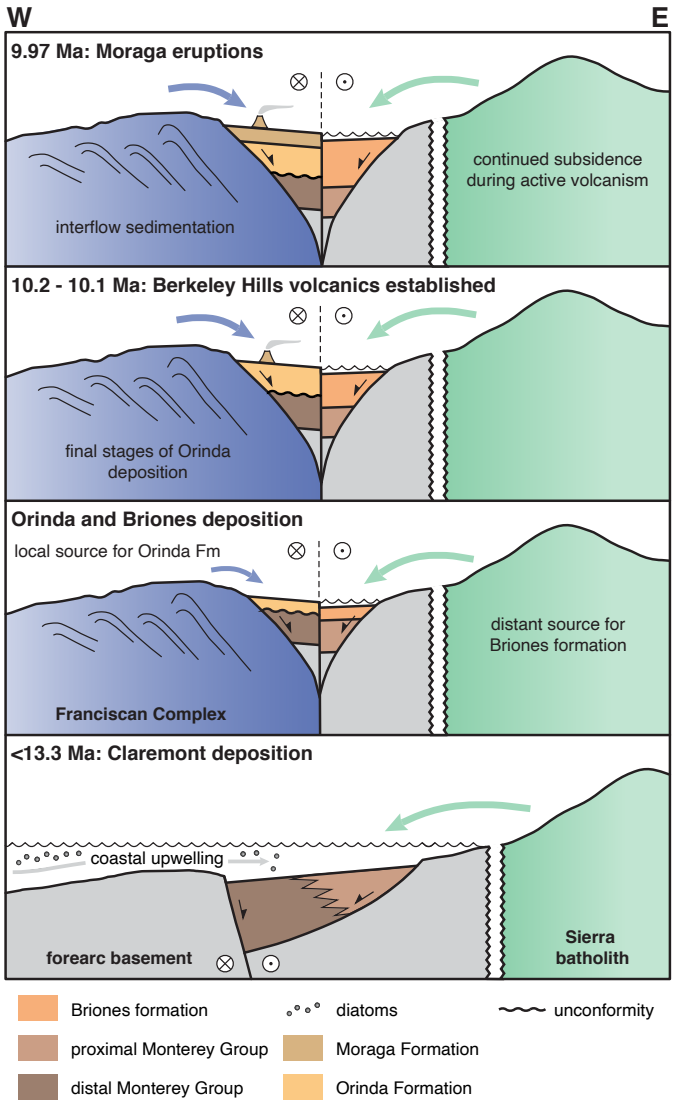

Figure 6. Simplified schematic illustration of sediment provenance and tectonic history of basin development associated with Miocene strata in the Berkeley Hills region. Basin geometry is characteristic of modeled transtensional strike-slip motion (Wu et al., 2009). The breaks between the forearc basement and Sierra batholith represent a large amount of distance. We interpret Claremont formation (Monterey Group) deposition to have occurred during initial regional transtension associated with the arrival of the Mendocino triple junction (Atwater and Stock, 1998). Zircon within the marine Claremont formation were dominantly sourced from the Sierra batholith. Uplift was followed by renewed subsidence leading to deposition of terrestrial sediments of the Orinda Formation, which were sourced from uplifted Franciscan Complex lithologies. Broadly time-equivalent marine sandstones of the Briones formation maintain the same Sierran sourced provenance as the Claremont formation. Slab-gap volcanism then initiated during ongoing subsidence leading to the eruption of the Moraga Formation volcanics during terminal Orinda Formation deposition.

further supported by sandstone petrography, where the relative proportion of polycrystalline quartz, sedimentary-metasedimentary rock fragments, and volcanic-metavolcanic rock fragments supports a switch from a dominant Sierran arc provenance for Monterey Group sandstones to a dominantly Franciscan or Great Valley Group provenance for the Contra Costa Group sandstones (Graham et al., 1984).

During Claremont formation deposition, the interpretation that terrestrial detritus was sourced dominantly from the Sierran arc is strongly

supported by the similarity in the detrital zircon spectra with the magmatic age compilation from the Sierra batholith (Figs. 3 and 4). The additional Miocene grains in the Claremont formation that enable the determination of a useful maximum depositional age may be best attributed to being sourced from the ancestral Cascade arc in the northern Sierra Nevada, as was interpreted by Gooley et al. (2021) for similar-aged zircon in the Hambre formation of the Monterey Group and the Briones formation of the Contra Costa Group. Zircon trace element data are consistent with the Gooley et al. (2021) interpretation of an ancestral Cascade arc being the source of Miocene zircon in the Claremont formation (Fig. 5). However, the lack of U/Yb versus Nb/Yb trace element data for slab-gap volcanics makes the uniqueness of this interpretation difficult to assess. It is also possible that these grains were sourced from slab-gap Coast Ranges volcanics to the south of the East Bay block that were transported along the margin. Detrital zircon age spectra of the lower Orinda Formation (Gooley et al., 2021) and the upper Orinda Formation from this study vary (Fig. 4). It is possible that the lower Orinda Formation exhibits a transitional age signature that more closely resembles that of the Claremont formation as a result of a shared sediment pathway to the east.

A simplified schematic and cartoon illustration of basin development and sedimentary provenance is shown in Figure 6. Here we illustrate our preferred interpretation that Claremont formation deposition occurred in an offshore transtensional basin, with terrestrial detritus dominantly sourced from the Sierra Nevada and upwelling nutrient-rich waters from offshore leading to diatom blooms that resulted in the deposition of siliceous sediment. Changing fault geometry along the margin would have led to redistribution of regional uplift and subsidence such that during terrestrial deposition of the Orinda Formation, there was an emergent highland of Franciscan Complex lithologies to the west that shed detritus into the basin. Such uplift of the Franciscan Complex could be attributed to a period of transpression as a result of a restraining bend in the fault system or a migrating stepover in the fault system (Wakabayashi et al., 2004; Wakabayashi, 2007). A period of sustained transtension—likely a product of a releasing bend in the fault system—permitted the conformable deposition of the Orinda, Moraga, Siesta, and Bald Peak Formations.

Stratigraphic correlations between fault-bound assemblages can be difficult because in addition to fault offset following deposition, basins deposited within a transform setting are commonly variably and diachronously formed. The shallow-marine Briones formation is interpreted to be time correlative to the Orinda Formation in a distinct fault-bound assemblage to the east (Graham et al., 1984; Chetelat, 1995). The Briones Formation has zircon dates and lithic grain compositions consistent with a dominant Sierran arc provenance associated with clastic sediment transport from the east (Fig. 4; Graham et al., 1984; Gooley et al., 2021). Onset of Briones formation deposition is given a range between 16 and 10 Ma based on vertebrate fossils in assemblage II (ages from Wagner, 1978; classification scheme based on Graymer, 2000). However, ages assigned to the Briones formation vary across fault-bound assemblages, given that deposition is proposed to have overlapped with deposition of the Orinda, Moraga, Siesta, and Bald Peak Formations of the Berkeley Hills in assemblages IV, VIII, IX, and X classification scheme based on Graymer (2000) and McDougall and Block (2014). A similar pattern applies to the Orinda Formation, where onset is interpreted to have occurred as early as 11.5 Ma and as late as 6.7 Ma, with younger sections in the east (Wagner et al., 2021). The overall relationship of deposition of the terrestrial Orinda Formation and that of the likely coeval shallow-marine Briones formation can be envisioned as a bay or inland sea, with Franciscan uplands being between the shallow-marine depocenter of the Briones and the open ocean (Graham et al., 1984).

Additional constraints on the timing of the passage of the Mendocino triple junction come from the timing of slab-gap volcanism. The eruption of the Moraga Tuff following the accumulation of ~150 m of basaltic lava flows constrains volcanism to have been ongoing ca. 9.9 Ma. The tuff clast within the uppermost Orinda Formation conglomerate, with an interpreted eruptive date of 10.094 ± 0.018 Ma, is likely associated with local Coast Ranges volcanism prior to the basalt eruptions recorded in the Berkeley Hills assemblage. That there is one antecrystic zircon within the Moraga Tuff (analysis z7) and two antecrystic zircon grains (z4 and z6) within the Orinda tuff clast with overlapping dates of ca. 10.13 Ma is suggestive of a shared magmatic system with similar subsurface crystallization histories prior to eruption (Fig. 2). In this context, the oldest antecrystic zircon grain within the Orinda tuff clast of 10.593 ± 0.019 Ma may constrain some of the earliest melt generation associated with the development of slab-gap volcanism in the region.

Quaternary volcanism in the Clear Lake region is occurring ~80 km south of the present-day southernmost edge of the subducting Juan de Fuca plate as placed by Atwater and Stock (1998). Reconstruction of the edge of the Juan de Fuca slab gives insight that this ~80 km distance between volcanism and the slab edge holds for the ca. 2.1 Ma initiation of the southern Clear Lake Volcanics as well (Fig. 7). There is a similar ~80 km distance between the slab edge ca. 12 Ma and the ca. 11.6 Ma initiation of the Quien Sabe Volcanics, indicating similarities in this aspect of the magmatic systems through time (Fig. 7). The migration rate of the slab edge of ~25 km/m.y. and distance of ~80 km from slab edge to volcanics gives a time lag of ~3.2 m.y. from initial establishment of transform system to onset of slab-gap volcanism. To consider the position of the Berkeley Hills assemblage relative to the past position of the Mendocino triple junction and the associated edge of the Juan de Fuca slab, the relative displacement of the Berkeley Hills assemblage relative to California's Central Valley needs to be considered. While the majority of right-lateral offset in the region has been associated with the Hayward fault, there is also displacement associated with faults to the east of the Hayward fault. Graymer et al. (2002) estimated that there has been ~75 km of offset of the Berkeley Hills assemblage relative to the Central Valley since ca. 10 Ma associated with these right-lateral fault systems; in contrast, the Quien Sabe Volcanics have not been translated. Taking this offset into account, the position of the Berkeley Hills assemblage at the time of ca. 10 Ma eruption of the Moraga Formation

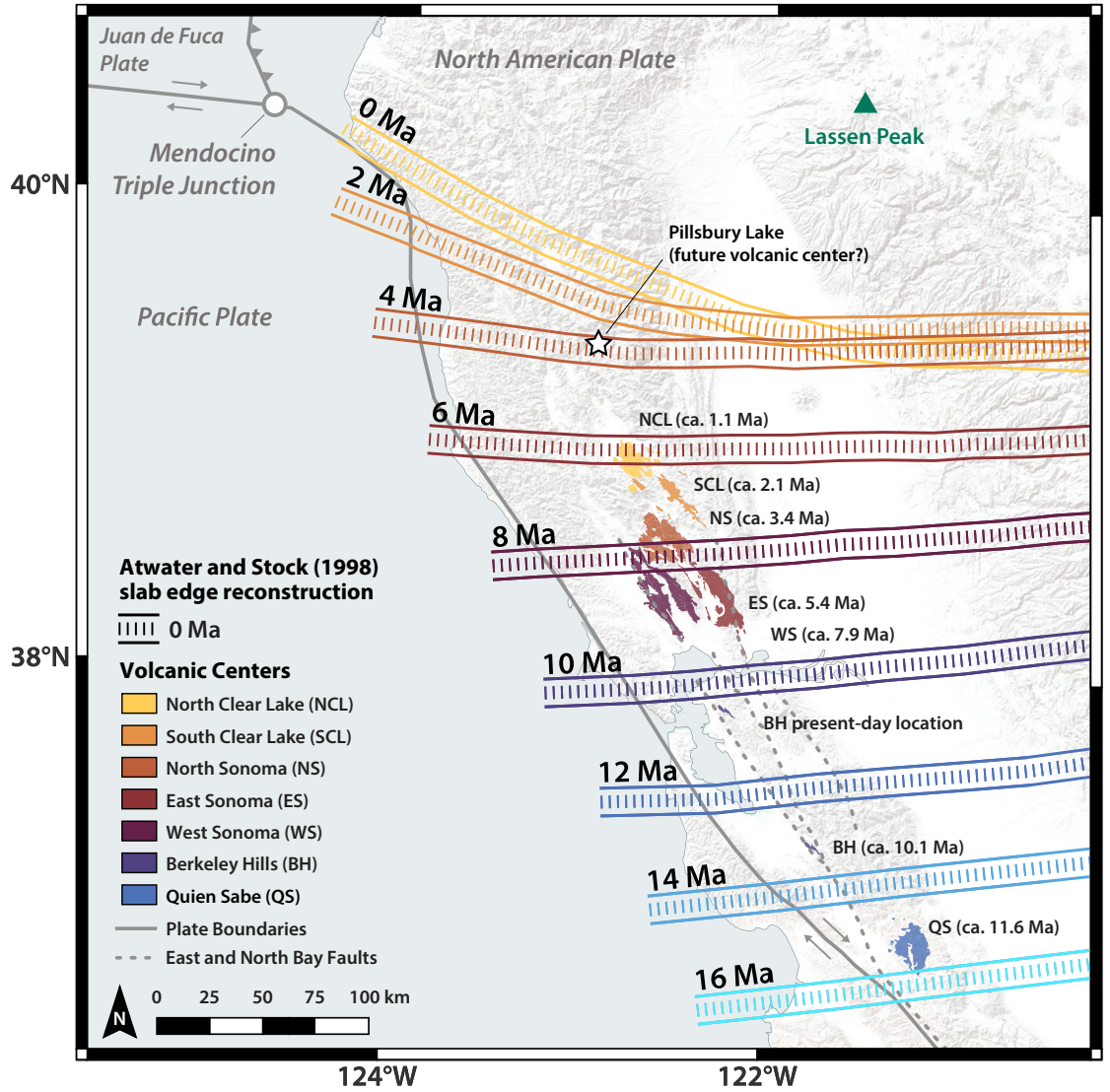

Figure 7. California Coast Ranges volcanic centers shown with the southern edge of the Juan de Fuca slab as reconstructed by Atwater and Stock (1998). Ages shown for volcanic centers correspond to the oldest radiometric dates and therefore the interpreted onset of volcanism. References for dates are: Quien Sabe Volcanics—Drinkwater et al. (1992); Berkeley Hills volcanics—this study; Sonoma Volcanics—Wagner et al. (2011); Clear Lake Volcanics—Donnelly-Nolan et al. (1981). Offset along faults associated with the Hayward-Calaveras fault system complicates the relative positions particularly for the west Sonoma Volcanics and the Berkeley Hills volcanics. Berkeley Hills volcanics (Moraga Bald Peak Formations) are reconstructed ~75 km to the south-southeast along the fault system following Graymer et al. (2002). Distance between the slab edge and coeval volcanic centers is ~80 km as seen geologically recently for the Clear Lake Volcanics back to ca. 12 Ma for the Quien Sabe Volcanics. A possible future location of volcanism as proposed by Levander et al. (1998) on the basis of interpreted crustal melt is shown at Pillsbury Lake. Lassen Peak is the southernmost volcano in the Cascades continental arc associated with ongoing subduction north of the Mendocino triple junction and is further away from the plate margin than the slab-gap Coast Ranges volcanics.

volcanics would have been ~80 km south of the edge of the Juan de Fuca plate as reconstructed at 10 Ma by Atwater and Stock (1998)—the same distance as there is between the plate edge and the present-day expression of slab-gap volcanism (Fig. 7). Such lagging magmatism in the wake of triple junction passage has been predicted through geodynamic modeling (Furlong, 1984) and incorporated into fault reconstructions (Wakabayashi, 1999). Given the time lag between the passage of the triple junction and surface volcanism resulting from slab-gap upwelling, the location of the Berkeley Hills assemblage would have experienced the effects of transform margin tectonics well before volcanism began. Considering the reconstructed position of the triple junction by Atwater and Stock (1998) and the offset interpreted by Graymer et al. (2002), the triple junction would have arrived slightly before 13 Ma. Given the maximum depositional age of <13.3 Ma within the Claremont formation, this timing is consistent with the Monterey Group strata of the Berkeley Hills assemblage being deposited in a basin that formed during the initial arrival of the transform boundary.

CONCLUSION

Transform margins have dynamic fault systems that can change over geologically short time scales, leading to time-varying subsidence and uplift. This study has constrained these transform dynamics, sometimes referred to as yo-yo tectonics, to have occurred in <3 m.y. New chronostratigraphic data from the Berkeley Hills assemblage support an interpretation that arrival of the transform margin to the modern day Bay Area region occurred by ca. 13 Ma and led to subsidence in which the marine deep-water sediments of the Claremont formation (Monterey Group) were deposited. Uplift followed by renewed subsidence led to deposition of terrestrial sediments of the Contra Costa Group, whose provenance requires transpressional uplift of a block dominated by Franciscan Complex lithologies to the west. Ca. 10 Ma slab-gap volcanism likely followed the onset of strike-slip tectonics in the region by several million years. Subsequent changes along the transform margin have translated the Berkeley Hills assemblage to the north, with contractional deformation uplifting it to form the present-day topography of the Berkeley Hills.

ACKNOWLEDGMENTS

We recognize that project research took place in the traditional, unceded territory of the Muwekma Ohlone Tribe. We thank the many University of California (UC) Berkeley students past and present whose study of these rocks has been inspirational for this study and George Brimhall for introducing Swanson-Hysell to the geology of the Berkeley Hills. We also thank James Pierce for providing integral field assistance, Nicolas Anderson for data analysis insight, John Grimsich for lab support and encouragement, Darin Schwartz for LA-ICP-MS assistance, and Mark Schmitz for access to the Boise State University geochronology lab. Conversations with Eliel Anttila on Monterey Group basin formation and chronostratigraphy along with Alan Deino on the comparison of Ar-Ar and U-Pb geochronology have been inspiring and informative. Project research was supported by the UC Berkeley Earth and Planetary Science Department Ramsden Fund and U.S. National Science Foundation grant EAR-1925990. Publication made possible in part by support from the Berkeley Research Impact Initiative, sponsored by the UC Berkeley Library. We thank two anonymous reviewers whose input has improved the manuscript in addition to David Fastovsky for editorial handling of the manuscript. We also gratefully acknowledge constructive reviews by Ryan Leary and Russell Graymer on an earlier version of the manuscript. All code associated with the data visualization and analysis conducted in this study as well as all associated data are available in an open GitHub repository associated with this work (https://github.com/Swanson-Hysell-Group/Gerasimov_Berkeley_Hills) that is also archived on Zenodo (https://doi.org/10.5281/zenodo.8006955).

REFERENCES CITED

Alroy, J., 2000, New methods for quantifying macroevolutionary patterns and processes: Paleobiology, v. 26, p. 707–733, https://doi.org/10.1666/0094-8373(2000)026<0707:NMFQMP>2.0.CO;2.

Atwater, T., 1970, Implications of plate tectonics for the Cenozoic tectonic evolution of western North America: Geological Society of America Bulletin, v. 81, p. 3513–3536, https://doi.org/10.1130/0016-7606(1970)81[3513:IOPTFT]2.0.CO;2.

Atwater, T., and Stock, J., 1998, Pacific–North America plate tectonics of the Neogene southwestern United States: An update: International Geology Review, v. 40, p. 375–402, https://doi.org/10.1080/00206819809465216.

Barron, J.A., 1986, Paleoceanographic and tectonic controls on deposition of the Monterey formation and related siliceous rocks in California: Palaeogeography, Palaeoclimatology, Palaeoecology, v. 53, p. 27–45, https://doi.org/10.1016/0031-0182(86)90037-4.

Barron, J.A., 1989, Diatom stratigraphy of the Monterey Formation and related rocks, San Jose 30′ by 60′ quadrangle, California. U.S. Geological Survey Open-File Report 89-565, 19 p., https://doi.org/10.3133/ofr89565.

Behl, R.J., 1999, Since Bramlette (1946): The Miocene Monterey Formation of California revisited, *in* Moores, E.M., Sloan, D., and Stout, D.L., eds., Classic Cordilleran Concepts: A View from California, Geological Society of America Special Paper 338, p. 301–313, https://doi.org/10.1130/0-8137-2338-8.301.

Benz, H.M., Zandt, G., and Oppenheimer, D.H., 1992, Lithospheric structure of northern California from teleseismic images of the upper mantle: Journal of Geophysical Research: Solid Earth, v. 97, p. 4791–4807, https://doi.org/10.1029/92JB00067.

Bero, D.A., Anfinson, O.A., and Raymond, L.A., 2020, New insights on Franciscan Complex geology, architecture, depositional age, and provenance for the western Mt. Tamalpais area, Marin County, California: International Geology Review, v. 63, p. 1563–1595, https://doi.org/10.1080/00206814.2020.1785338.

Blake, M.C., Jr., Campbell, R.H., Dibblee, T.W., Jr., Howell, D.G., Nilsen, T.H., Normark, W.R., Vedder, J.C., and Silver, E.A., 1978, Neogene basin formation in relation to plate-tectonic evolution of San Andreas fault system, California: American Association of Petroleum Geologists Bulletin, v. 62, p. 344–372, https://doi.org/10.1306/C1EA484C-16C9-11D7-8645000102C1865D.

Buising, A.V., and Walker, J.P., 1995, Preliminary palinspastic paleogeographic reconstructions for the greater San Francisco Bay area, 15 Ma–5 Ma, *in* Sanginés, E.M., Andersen, D.W., and Buising, A.B., eds., Recent Geologic Studies in the San Francisco Bay Area: Pacific Section, Society of Economic Paleontologists and Mineralogists, v. 76, p. 141–159.

Boyd, D.L., Walton, G., and Trainor-Guitton, W., 2020, Geostatistical estimation of Ground Class prior to and during excavation for the Caldecott Tunnel Fourth Bore project: Tunnelling and Underground Space Technology, v. 100, https://doi.org/10.1016/j.tust.2020.103391.

Chapman, A.D., Saleeby, J.B., Wood, D.J., Piasecki, A., Kidder, S., Ducea, M.N., and Farley, K.A., 2012, Late Cretaceous gravitational collapse of the southern Sierra Nevada batholith, California: Geosphere, v. 8, p. 314–341, https://doi.org/10.1130/GES00740.1.

Chetelat, G.F., 1995, Provenance of the upper-Miocene Briones formation in the central Diablo Range, California [M.S. thesis]: San Jose, California, San Jose State University, 130 p.

Christie-Blick, N., and Biddle, K.T., 1985, Deformation and basin formation along strike-slip faults, *in* Biddle, K.T., and Christie-Blick, N., eds., Strike-Slip Deformation, Basin Formation, and Sedimentation: Society of Economic Paleontologists and Mineralogists Special Publication 37, p. 1–34, https://doi.org/10.2110/pec.85.37.0001.

Cole, R.B., and Basu, A.R., 1995, Nd-Sr isotopic geochemistry and tectonics of ridge subduction and middle Cenozoic volcanism in western California: Geological Society of America Bulletin, v. 107, p. 167–179, https://doi.org/10.1130/0016-7606(1995)107<0167:NSIGAT>2.3.CO;2.

Creely, S., Savage, D.E., and Ogle, B.A., 1982, Stratigraphy of upper Tertiary nonmarine rocks of central Contra Costa Basin, California, *in* Ingersoll, R.V., and Woodborne, M.O., eds., Cenozoic Nonmarine Deposits of California and Arizona: Pacific Section, Society of Economic Paleontologists and Mineralogists, p. 11–22.

Crowell, J.C., 1974, Origin of late Cenozoic basins in southern California, *in* Dickinson, W.R., ed., Tectonics and Sedimentation: Society of Economic Paleontologists and Mineralogists Special Publication 22, p. 190–204, https://doi.org/10.2110/pec.74.22.0190.

Curtis, G.H., 1989, Berkeley Hills, *in* Wahrhaftig, C., and Sloan, D., eds., Geology of San Francisco and Vicinity: American Geophysical Union Field Trip Guidebook 105, p. 47–49.

DePaolo, D.J., and Finger, K.L., 1991, High-resolution strontium-isotope stratigraphy and biostratigraphy of the Miocene Monterey Formation, central California: Geological Society of America Bulletin, v. 103, p. 112–124, https://doi.org/10.1130/0016-7606(1991)103<0112:HRSISA>2.3.CO;2.

Dickinson, W.R., 1981, Plate tectonics and the continental margin of California, *in* Ernst, W.G., ed., The Geotectonic Development of California: Rubey Volume 1: Englewood Cliffs, New Jersey, Prentice-Hall, p. 1–28.

Donnelly-Nolan, J.M., Hearn, B.C., Jr., Curtis, G.H., and Drake, R.E., 1981, Geochronology and evolution of the Clear Lake Volcanics, *in* McLaughlin, R.J., and Donnelly-Nolan, J.M., eds., Research in the Geysers–Clear Lake Geothermal Area, Northern California: U.S. Geological Survey Professional Paper 1141, p. 47–60.

Drinkwater, J.L., Sorg, D.H., and Russell, P.C., 1992, Geologic map showing age and mineralization of the Quien Sabe Volcanics, Mariposa Creek quadrangle, west-central California: U.S. Geological Survey Miscellaneous Field Studies Map MF-2200, scale 1:24,000, https://doi.org/10.3133/mf2200.

Estes, P., Gavigan, C., Graham, S., McCloy, C., Weber, L., and Hitzman, M., 1983, Orinda and Moraga Formations at eastern portal of Caldecott Tunnel, *in* Cherven, V.B., and Graham, S.A., eds., Geology and Sedimentology of the Southwestern Sacramento Basin and East Bay Hills: Los Angeles, Pacific Section, Society of Economic Paleontologists and Mineralogists, p. 89–92.

Fay, R.P., and Fleck, R.J., 2014, New age constraints on the late Miocene Orinda Formation in the southern Contra Costa Basin: Geological Society of America Abstracts with Programs, v. 46, no. 6, p. 551.

Flower, B.P., and Kennett, J.P., 1993, Relations between Monterey Formation deposition and middle Miocene global cooling: Naples Beach section: California Geology, v. 21, p. 877–880, https://doi.org/10.1130/0091-7613(1993)021<0877:RBMFDA>2.3.CO;2.

Fox, K.F., Fleck, R.J., Curtis, G.H., and Meyer, C.E., 1985, Implications of the northwestwardly younger age of the volcanic rocks of west-central California: Geological Society of America Bulletin, v. 96, p. 647–654, https://doi.org/10.1130/0016-7606(1985)96<647:IOTNYA>2.0.CO;2.

Furlong, K.P., 1984, Lithospheric behavior with triple junction migration: An example based on the Mendocino triple junction: Physics of the Earth and Planetary Interiors, v. 36, p. 213–223, https://doi.org/10.1016/0031-9201(84)90047-5.

Furlong, K.P., and Schwartz, S.Y., 2004, Influence of the Mendocino triple junction on the tectonics of coastal California: Annual Review of Earth and Planetary Sciences, v. 32, p. 403–433, https://doi.org/10.1146/annurev.earth.32.101802.120252.

Gooley, J.T., Grove, M., and Graham, S.A., 2021, Tectonic evolution of the central California margin as reflected by detrital zircon composition in the Mount Diablo region, *in* Sullivan, R., Sloan, D., Unruh, J.R., and Schwartz, D.P., eds., Regional Geology of Mount Diablo, California: Its Tectonic Evolution on the North America Plate Boundary: Geological Society of America Memoir 217, p. 305–329, https://doi.org/10.1130/2021.1217(14).

Graham, S.A., McCloy, C., Hitzman, M., Ward, R., and Turner, R., 1984, Basin evolution during change from convergent to transform continental margin in central California: American Association of Petroleum Geologists Bulletin, v. 68, p. 233–249, https://doi.org/10.1306/AD460A03-16F7-11D7-8645000102C1865D.

Graymer, R.W., 2000, Geologic map and map database of the Oakland metropolitan area, Alameda, Contra Costa, and San Francisco Counties, California: U.S. Geological Survey Miscellaneous Field Studies Map MF-2342, scale 1:50,000, https://doi.org/10.3133/mf2342.

Graymer, R.W., Sarna-Wojcicki, A.M., Walker, J.P., McLaughlin, R.J., and Fleck, R.J., 2002, Controls on timing and amount of right-lateral offset on the East Bay fault system, San Francisco Bay region, California: Geological Society of America Bulletin, v. 114, p. 1471–1479, https://doi.org/10.1130/0016-7606(2002)114<1471:COTAAO>2.0.CO;2.

Grimes, C.B., Wooden, J.L., Cheadle, M.J., and John, B.E., 2015, "Fingerprinting" tectono-magmatic provenance using trace elements in igneous zircon: Contributions to Mineralogy and Petrology, v. 170, 46, https://doi.org/10.1007/s00410-015-1199-3.

Grimsich, J.L., Scott, G.R., Swisher, C.C., III, and Curtis, G.H., 1996, Paleomagnetism and $^{40}Ar/^{39}Ar$ dating of the Miocene Contra Costa Group, Berkeley Hills, California: Eos (Transactions, American Geophysical Union), v. 77, p. 165.

Hammersley, L., and DePaolo, D.J., 2006, Isotopic and geophysical constraints on the structure and evolution of the Clear Lake volcanic system: Journal of Volcanology and Geothermal Research, v. 153, p. 331–356, https://doi.org/10.1016/j.jvolgeores.2005.12.003.

Hengesh, J.V., and Wakabayashi, J., 1995, Dextral translation and progressive emergence of the Pleistocene Merced Basin and implications for timing of initiation of the San Francisco Peninsula segment of the San Andreas fault, *in* Sanginés, E.M., Andersen, D.W., and Buising, A.V., eds., Recent Geologic Studies in the San Francisco Bay Area: Pacific Section, Society of Economic Paleontologists and Mineralogists, v. 76, p. 47–54.

Hiess, J., Condon, D.J., McLean, N., and Noble, S.R., 2012, $^{238}U/^{235}U$ systematics in terrestrial uranium-bearing minerals: Science, v. 335, p. 1610–1614, https://doi.org/10.1126/science.1215507.

Hill, J.M., 1979, Stratigraphy and paleoenvironment of the Miocene Monterey Group in the East San Francisco Bay region, California: U.S. Geological Survey Open-File Report 79-1570, 75 p., 4 sheets, https://doi.org/10.3133/ofr791570.

Hodgin, E.B., Swanson-Hysell, N.L., DeGraff, J.M., Kylander-Clark, A.R.C., Schmitz, M.D., Turner, A.C., Zhang, Y.M., and Stolper, D.A., 2022, Final inversion of the Midcontinent Rift during the Rigolet Phase of the Grenvillian Orogeny: Geology, v. 50, p. 547–551, https://doi.org/10.1130/G49439.1.

Idleman, L., Cosca, M.A., Heizler, M.T., Thomson, S.N., Teyssier, C., and Whitney, D.L., 2014, Tectonic burial and exhumation cycles tracked by muscovite and K-feldspar $^{40}Ar/^{39}Ar$ thermochronology in a strike-slip fault zone, central Turkey: Tectonophysics, v. 612–613, p. 134–146, https://doi.org/10.1016/j.tecto.2013.12.003.

Irwin, W.P., 1990, Geology and plate-tectonic development, *in* Wallace, R., ed., The San Andreas Fault System, California: U.S. Geological Survey Professional Paper 1515, p. 61–80.

Jachens, R.C., and Griscom, A., 1983, Three-dimensional geometry of the Gorda Plate beneath northern California: Journal of Geophysical Research: Solid Earth, v. 88, p. 9375–9392, https://doi.org/10.1029/JB088iB11p09375.

Jaffey, A.H., Flynn, K.F., Glendenin, L.E., Bentley, W.C., and Essling, A.M., 1971, Precision measurement of half-lives and specific activities of ^{235}U and ^{238}U: Physical Review C, v. 4, p. 1889–1906, https://doi.org/10.1103/PhysRevC.4.1889.

Johnson, C.M., and O'Neil, J.R., 1984, Triple junction magmatism: A geochemical study of Neogene volcanic rocks in western California: Earth and Planetary Science Letters, v. 71, p. 241–262, https://doi.org/10.1016/0012-821X(84)90090-6.

Jones, D.L., and Curtis, G.H., 1991, Guide to the geology of the Berkeley Hills, central Coast Ranges, California, *in* Sloan, D., and Wagner, D.L., eds., Geologic Excursions in Northern California: San Francisco to the Sierra Nevada: California Division of Mines and Geology Special Publication 109, p. 63–73.

Kleinpell, R.M., 1938, Miocene stratigraphy of California: Tulsa, Oklahoma, American Association of Petroleum Geologists, 450 p.

Lachenbruch, A.H., and Sass, J.H., 1980, Heat flow and energetics of the San Andreas Fault Zone: Journal of Geophysical Research: Solid Earth, v. 85, p. 6185–6222, https://doi.org/10.1029/JB085iB11p06185.

Lawson, A.C., 1914, Description of the San Francisco district, *in* San Francisco Folio, California, Tamalpais, San Francisco, Concord, San Mateo, and Haywards Quadrangles: U.S. Geological Survey Geologic Atlas Folio 193, 24 p., https://doi.org/10.3133/gf193.

Levander, A., Henstock, T.J., Meltzer, A.S., Beaudoin, B.C., Trehu, A.M., and Klemperer, S.L., 1998, Fluids in the lower crust following Mendocino triple junction migration: Active basaltic intrusion?: Geology, v. 26, p. 171–174, https://doi.org/10.1130/0091-7613(1998)026<0171:FITLCF>2.3.CO;2.

Liu, K.J., Levander, A., Zhai, Y.B., Porritt, R.W., and Allen, R.M., 2012, Asthenospheric flow and lithospheric evolution near the Mendocino Triple Junction: Earth and Planetary Science Letters, v. 323–324, p. 60–71, https://doi.org/10.1016/j.epsl.2012.01.020.

Ludington, S., Moring, B.C., Miller, R.J., Stone, P.A., Bookstrom, A.A., Bedford, D.R., Evans, J.G., Haxel, G.A., Nutt, C.J., Flyn, K.S., and Hopkins, M.J., 2005, Preliminary integrated geologic map databases for the United States, Western States: California, Nevada, Arizona, Washington, Oregon, Idaho, and Utah: U.S. Geological Survey Open-File Report 2005-1305, scale 1:500,000, https://doi.org/10.3133/ofr20051305.

Mattinson, J.M., 2005, Zircon U-Pb chemical abrasion ("CA-TIMS") method: Combined annealing and multi-step partial dissolution analysis for improved precision and accuracy of zircon ages: Chemical Geology, v. 220, no. 1–2, p. 47–66, https://doi.org/10.1016/j.chemgeo.2005.03.011.

McDougall, K., and Block, D.L., 2014, Digital database of microfossil localities in Alameda and Contra Costa Counties, California: U.S. Geological Survey Scientific Investigations Report 2014-5120, https://doi.org/10.3133/sir20145120.

Mertzman, S., 2000, K-Ar results from the southern Oregon–northern California Cascade Range: Oregon Geology, v. 62, p. 99–122.

Miller, K.G., Browning, J.V., Schmelz, W.J., Kopp, R.E., Mountain, G.S., and Wright, J.D., 2020, Cenozoic sea-level and cryospheric evolution from deep-sea geochemical and continental margin records: Science Advances, v. 6, https://doi.org/10.1126/sciadv.aaz1346.

Murray, R.W., Jones, D.L., and Buchholtz ten Brink, M.R., 1992, Diagenetic formation of bedded chert: Evidence from chemistry of the chert-shale couplet: Geology, v. 20, p. 271–274, https://doi.org/10.1130/0091-7613(1992)020<0271:DFOBCE>2.3.CO;2.

Nilsen, T.H., and Sylvester, A.G., 1999, Strike-slip basins: Part 1: The Leading Edge, v. 18, p. 1146–1152, https://doi.org/10.1190/1.1438170.

Page, B.M., 1950, Geology of the Broadway Tunnel, Berkeley Hills, California: Economic Geology, v. 45, p. 142–166, https://doi.org/10.2113/gsecongeo.45.2.142.

Pisciotto, K.A., and Garrison, R.E., 1981, Lithofacies and depositional environments of the Monterey Formation, California, *in* Garrison, R.E., and Douglas, R.G., eds., The Monterey Formation and Related Siliceous Rocks of California: Los Angeles, Pacific Section, Society of Economic Paleontologists and Mineralogists, p. 97–122.

Poust, A.W., 2017, First report of fossil turtle eggshell west of the Colorado Plateau: Historical Biology, v. 29, p. 473–479, https://doi.org/10.1080/08912963.2016.1189911.

Powell, C.L., II, Clites, E.C., and Poust, A.W., 2019, Miocene marine macropaleontology of the fourth bore Caldecott Tunnel excavation, Berkeley Hills, Oakland, California, USA: PaleoBios, v. 36, https://doi.org/10.5070/P9361044567.

Raffi, I., Wade, B.S., Pälike, H., Beu, A.G., Cooper, R., Crundwell, M.P., Krijgsman, W., Moore, T., Raine, I., Sardella, R., and Vernyhorova, Y.V., 2020, The Neogene Period, *in* Gradstein, F.M., Ogg, J.G., Schmitz, M.D., and Ogg, G.M., eds., Geologic Time Scale 2020: Amsterdam, Elsevier, v. 2, p. 1141–1215, https://doi.org/10.1016/B978-0-12-824360-2.00029-2.

Saylor, J.E., and Sundell, K.E., 2016, Quantifying comparison of large detrital geochronology data sets: Geosphere, v. 12, p. 203–220, https://doi.org/10.1130/GES01237.1.

Schmitz, M.D., and Schoene, B., 2007, Derivation of isotope ratios, errors, and error correlations for U-Pb geochronology using ^{205}Pb-^{235}U-(^{233}U)-spiked isotope dilution thermal ionization mass spectrometric data: Geochemistry, Geophysics, Geosystems, v. 8, no. 8, https://doi.org/10.1029/2006GC001492.

Sharman, G.R., Graham, S.A., Grove, M., Kimbrough, D.L., and Wright, J.E., 2015, Detrital zircon provenance of the Late Cretaceous–Eocene California forearc: Influence of Laramide low-angle subduction on sediment dispersal and paleogeography: Geological Society of America Bulletin, v. 127, p. 38–60, https://doi.org/10.1130/B31065.1.

Sharman, G.R., Sharman, J.P., and Sylvester, Z., 2018, detritalPy: A python-based toolset for visualizing and analysing detrital geo-thermochronologic data: The Depositional Record, v. 4, p. 202–215, https://doi.org/10.1002/dep2.45.

Stacey, J.S., and Kramers, J.D., 1975, Approximation of terrestrial lead isotope evolution by a two-stage model: Earth and Planetary Science Letters, v. 26, no. 2, p. 207–221, https://doi.org/10.1016/0012-821X(75)90088-6.

Sullivan, R., Fay, R.P., Schaefer, C., Deino, A., and Edwards, S.W., 2021, Neogene volcanism on the eastside of Mount Diablo, Contra Costa County, California, *in* Sullivan, R., Sloan, D., Unruh, J.R., and Schwartz, D.P., eds., Regional Geology of Mount Diablo, California: Its Tectonic Evolution on the North America Plate Boundary: Geological Society of America Memoir 217, p. 201–228, https://doi.org/10.1130/2021.1217(11).

Surpless, K.D., Clemens-Knott, D., Barth, A.P., and Gevedon, M., 2019, A survey of Sierra Nevada magmatism using Great Valley detrital zircon trace-element geochemistry: View from the forearc: Lithosphere, v. 11, p. 603–619, https://doi.org/10.1130/L1059.1.

Umhoefer, P.J., Whitney, D.L., Teyssier, C., Fayon, A.K., Casale, G., and Heizler, M.T., 2007, Yo-yo tectonics in a wrench zone, Central Anatolian fault zone, Turkey, *in* Roeske, S.M., Till, A.B., Foster, D.A., and Sample, J.C., eds., Exhumation Associated with Continental Strike-Slip Fault Systems: Geological Society of America Special Paper 434, p. 35–57, https://doi.org/10.1130/2007.2434(03).

Wagner, D.L., Saucedo, G.J., Clahan, K.B., Fleck, R.J., Langenheim, V.E., McLaughlin, R.J., Sarna-Wojcicki, A.M., Allen, J.R., and Deino, A.L., 2011, Geology, geochronology, and paleogeography of the southern Sonoma volcanic field and adjacent areas, northern San Francisco Bay region, California: Geosphere, v. 7, p. 658–683, https://doi.org/10.1130/GES00626.1.

Wagner, J.R., 1978, Late Cenozoic history of the Coast Ranges east of San Francisco Bay [Ph.D. thesis]: Berkeley, University of California, 322 p.

Wagner, J.R., Deino, A., Edwards, S.W., Sarna-Wojcicki, A.M., and Wan, E., 2021, Miocene stratigraphy and structure of the East Bay Hills, California, *in* Sullivan, R., Sloan, D., Unruh, J.R., and Schwartz, D.P., eds., Regional Geology of Mount Diablo, California: Its Tectonic Evolution on the North America Plate Boundary: Geological Society of America Memoir 217, p. 331–391, https://doi.org/10.1130/2021.1217(15).

Wakabayashi, J., 1999, Distribution of displacement on and evolution of a young transform fault system: The northern San Andreas fault system, California: Tectonics, v. 18, p. 1245–1274, https://doi.org/10.1029/1999TC900049.

Wakabayashi, J., 2007, Stepovers that migrate with respect to affected deposits: Field characteristics and speculation on some details of their evolution, *in* Cunningham, W.D., and Mann, P., eds., Tectonics of Strike-Slip Restraining and Releasing Bends: Geological Society of London Special Publication 290, p. 169–188, https://doi.org/10.1144/SP290.4.

Wakabayashi, J., 2015, Anatomy of a subduction complex: Architecture of the Franciscan Complex, California, at multiple length and time scales: International Geology Review, v. 57, p. 669–746, https://doi.org/10.1080/00206814.2014.998728.

Wakabayashi, J., Hengesh, J.V., and Sawyer, T.L., 2004, Four-dimensional transform fault processes: Progressive evolution of step-overs and bends: Tectonophysics, v. 392, p. 279–301, https://doi.org/10.1016/j.tecto.2004.04.013.

Woodburne, M.O, Macfadden, B.J., and Skinner, M.F., 1981, The North American *Hipparion* Datum and implications for the Neogene of the Old World: Geobios, v. 14, p. 493–524, https://doi.org/10.1016/S0016-6995(81)80124-6.

Woodcock, N.H., 2004, Life span and fate of basins: Geology, v. 32, p. 685–688, https://doi.org/10.1130/G20598.1.

Wu, J.E., McClay, K., Whitehouse, P., and Dooley, T., 2009, 4D analogue modelling of transtensional pull-apart basins: Marine and Petroleum Geology, v. 26, p. 1608–1623, https://doi.org/10.1016/j.marpetgeo.2008.06.007.

Xie, X.Y., and Heller, P.L., 2009, Plate tectonics and basin subsidence history: Geological Society of America Bulletin, v. 121, p. 55–64, https://doi.org/10.1130/B26398.1.

Zandt, G., and Furlong, K.P., 1982, Evolution and thickness of the lithosphere beneath coastal California: Geology, v. 10, p. 376–381, https://doi.org/10.1130/0091-7613(1982)10<376:EATOTL>2.0.CO;2.